Received: 3 April 2023 | Revised: 18 May 2023 | Accepted: 2 June 2023

DOI: 10.1111/pce.14647

DATA INSIGHT

Plant, Cell & Environment WILEY

Integrative time-scale and multi-*omics* analysis of host responses to viroid infection

Joan Márquez-Molins[1,2] | Pascual Villalba-Bermell[1] | Julia Corell-Sierra[1] | Vicente Pallás[2] | Gustavo Gomez[1]

[1]Department of Molecular Interactions and Regulation, Institute for Integrative Systems Biology (I2SysBio), Consejo Superior de Investigaciones Científicas (CSIC), Universitat de València (UV), Parc Científic, Paterna, Spain

[2]Department of Virologia Molecular y Evolutiva de Plantas, Instituto de Biología Molecular y Celular de Plantas (IBMCP), Consejo Superior de Investigaciones Científicas (CSIC), Universitat Politècnica de València, Valencia, Spain

Correspondence

Gustavo Gomez, Department of Molecular Interactions and Regulation, Instituto de Biología Integrativa de Sistemas (I2SysBio), Consejo Superior de Investigaciones Científicas (CSIC) - Universitat de València (UV), Parc Científic UV, Catedrático Agustín Escardino 9, Paterna, 46980 Valencia, Spain.
Email: gustavo.gomez@csic.es

Funding information

Generalitat Valenciana; Agencia Estatal de Investigación

Abstract

Viroids are circular RNAs of minimal complexity compelled to subvert plant-regulatory networks to accomplish their infectious process. Studies focused on the response to viroid-infection have mostly addressed specific regulatory levels and considered specifics infection-times. Thus, much remains to be done to understand the temporal evolution and complex nature of viroid-host interactions. Here we present an integrative analysis of the temporal evolution of the genome-wide alterations in cucumber plants infected with hop stunt viroid (HSVd) by integrating differential host transcriptome, sRNAnome and methylome. Our results support that HSVd promotes the redesign of the cucumber regulatory-pathways predominantly affecting specific regulatory layers at different infection-phases. The initial response was characterised by a reconfiguration of the host-transcriptome by differential exon-usage, followed by a progressive transcriptional downregulation modulated by epigenetic changes. Regarding endogenous small RNAs, the alterations were limited and mainly occurred at the late stage. Significant host-alterations were predominantly related to the downregulation of transcripts involved in plant-defence mechanisms, the restriction of pathogen-movement and the systemic spreading of defence signals. We expect that these data constituting the first comprehensive temporal-map of the plant-regulatory alterations associated with HSVd infection could contribute to elucidate the molecular basis of the yet poorly known host-response to viroid-induced pathogenesis.

KEYWORDS

epigenetic epidemiology, global response to biotic stress, host transcriptional regulation in response to pathogens, systems biology and diseases, viroid-host interactions

Joan Márquez-Molins and Pascual Villalba-Bermell have equal contribution.

1 | INTRODUCTION

Viroids (the smallest infectious agents known to date) comprise an intriguing group of plant pathogens affecting a varied range of hosts worldwide. These sub-viral pathogens are classified into two families, *Pospiviroidae*, whose replication takes place in the nucleus, and *Avsunviroidae*, exhibiting chloroplastic replication (Di Serio et al., 2017). As naked circular RNAs, viroids are compelled to closely interact with diverse (many yet unknown) host factors to fulfill their infectious cycle in the infected plants (Adkar-Purushothama & Perreault, 2020; Ding, 2009; Gómez and Pallás, 2013). However, how these pathogenic RNAs alter the host development and physiology, inducing disease symptoms, is still an unsolved question (Adkar-Purushothama & Perreault, 2020; Gago-Zachert, 2016; Navarro, Flores, et al., 2021).

In general, plants respond to stress conditions (including pathogen infection) through a complex reprogramming of their transcriptional activity. Gene regulation is a complex process modulated by a series of coordinated events involving multiple control layers such as: epigenetic modifications, gene expression and RNA interference (RNAi) (Annacondia et al., 2018; Baulcombe & Dean, 2014; Yaish, 2017). These different regulatory levels have been categorised as stress-responsive structures termed as Environmental Gene Regulatory Influence Networks (EGRINs) (Wilkins et al., 2016). Increasing evidence indicate that viroids can subvert different host-EGRINs and consequently promote the emergence of the phenotypic alterations recognised (in certain viroid-host interactions) as symptoms. In this regard, diverse studies have supported the notion that during the infectious process, viroids promote significant alterations in diverse plant regulatory pathways (Adkar-Purushothama & Perreault, 2020; Aviña-Padilla et al., 2022; Navarro, Flores, et al., 2021).

It has been proposed that viroids (presumably because of the highly compacted and structured genomic circular RNA), are resistant to degradation mediated by RNA-silencing (Elena et al., 2009; Gómez & Pallás, 2007; Itaya et al., 2007). However, early reports showed that viroid-derived sRNAs (vd-sRNAs) (arising probably from the DCL-mediated processing of replication intermediates) are detected in plants infected by members of both nuclear and chloroplastic families (Itaya et al., 2001; Martínez de Alba et al., 2002; Papaefthimiou et al., 2001), evidencing that certain biological forms (probably replication intermediates) of members of both families are targets of the host RNA silencing machinery. Although multiple studies have confirmed the association between viroid infection and accumulation of vd-sRNAs, their biogenesis still remains elusive (Di Di Serio et al., 2023). Also related to viroid-infection and RNA-silencing, alterations in the accumulation of certain endogenous microRNAs (miRNAs) have been reported in diverse viroid-host interactions (Diermann et al., 2010; Hadjieva et al., 2021; Lavagi-Craddock et al., 2021; Navarro, Gisel, et al., 2021; Owens et al., 2012; Sanz-Carbonell et al., 2019, 2020; Tsushima et al., 2015).

Modulation (in both positive and/or negative sense) of gene expression constitutes the core of the plant response to abiotic and biotic stress conditions (Wang et al., 2020; Waters et al., 2017). Changes at the transcriptomic level have been described in several plants infected by viroids of both *Pospiviroidae* and *Avsunviroidae* families (Aviña-Padilla et al., 2018; Góra-Sochacka et al., 2019; Herranz et al., 2013; Kappagantu et al., 2017; Katsarou et al., 2016; Rizza et al., 2012; Štajner et al., 2019; Xia et al., 2017). These studies have revealed alterations in genes related to defence, response to stress, hormone homeostasis and signalling, biosynthesis of cell wall compounds, and RNA metabolism (Adkar-Purushothama and Perreault, 2020).

A growing body of evidence points toward the existence of a close interplay between infection and epigenetic alterations in the host (plant or animal) genome (Annacondia et al., 2018; Wang et al., 2019). Consequently, epigenetic epidemiology has emerged as a promising area for future research on infectious diseases (Gómez-Díaz et al., 2012). Recent studies have evidenced dynamic changes in host DNA methylation patterns upon viroid infection in both somatic (Castellano, Pallas, et al., 2016; Lv et al., 2016; Martinez et al., 2014; Sečnik et al., 2022; Torchetti et al., 2016) and reproductive (Castellano, Martinez, et al., 2016) tissues. The changes of the host-genome epigenetic regulation have been connected (in infected cucumber plants) with viroid recruiting and functionally subverting the host HISTONE DEACETYLASE 6 (HDA6) (Castellano, Pallas, et al., 2016). Alteration of the host plant methylome has been also described to occur in response to infection by viruses (Corrêa et al., 2020) and bacteria (Deleris et al., 2016), supporting that regulation of host DNA methylation may be part of an evolutionary conserved immune response in plants (Zhu et al., 2016).

The above-described findings show how the advent of high-throughput sequencing technologies has favoured the study of the viroid-host interactions at a molecular level. However, such experimental approaches have been generally centred on the analysis of the viroid-induced changes at a single host-regulatory level and/or considering infection times mainly correlated to advanced disease stages (Hadjieva et al., 2021; Štajner et al., 2019; Zhang et al., 2020). Therefore, our knowledge about the functional diversity and temporal dynamics of the global plant response to viroid infection is scarce (Adkar-Purushothama & Perreault, 2020).

Here we have performed an integrative analysis of the timing and intensity of the genome-wide alterations in cucumber (*Cucumis sativus*) plants in response to hop stunt viroid (HSVd) infection (Marquez-Molins et al., 2021). Beside being the most polyphagous viroid described at the moment (Marquez-Molins et al., 2021), the use of the pathogenic model HSVd/cucumber has provided a considerable knowledge about the replication (Castellano, Pallas, et al., 2016), systemic movement (Gómez & Pallás, 2001; Gómez & Pallás, 2004), and pathogenesis (Castellano, Martinez, et al., 2016) of the viroids, as well as its interaction with host epigenetic mechanisms (Castellano, Martinez, et al., 2016; Castellano, Pallas, et al., 2016; Martinez et al., 2014). Our study has been focused on the temporal dynamics (at three infection time-points) of the plant response to viroid infection at three different regulatory levels of the gene expression network: (i) RNAi, (ii) gene expression and (iii) genomic

cytosine methylation. Our results indicate that HSVd infection promotes a dynamic redesign of the cucumber regulatory pathways that affects these regulatory layers distinctively depending on the infection phase.

2 | MATERIALS AND METHODS

2.1 | Viroid infection and sample collection

Cucumber plants cv. Marketer at cotyledon stage were inoculated with HSVd (Y09352.1) as previously described (Marquez-Molins et al., 2019). Both cotyledons were agro-infiltrated with a culture of *Agrobacterium tumefaciens* strain C58 with one of optical density, harboring pMD201t-HSVd or empty vector, diluted in infiltration buffer (MES 0.1 M, MgCl2 0.1 M). Plants were kept in a photoperiod of 16 h under visible light and 30°C (light)/25°C (darkness). The second leaf after the apex was collected at 10-, 17- and 24-day post inoculation (dpi). Each bio-replicate consisted of the leaves from three plants and for each time-point three bio-replicates were sampled of mock and HSVd infected plants.

2.2 | DNA and RNA extraction and library preparation

Total RNA was extracted using TRIzol reagent (Life Technologies) following the manufacturer instructions. Genomic DNA was extracted using a CTAB-based extraction method as previously described (Healey et al., 2014). All libraries were constructed by Novogene Europe according to their standard procedures, including the previous steps of messenger RNA (mRNA) purification with oligo (dT) beads sRNA purification by size selection.

2.3 | Small RNA sequencing and analysis

sRNA libraries were sequenced by single end (50 bp). The resulting reads were adapter trimmed and filtered on quality by Cutadapt v2.8 (Martin, 2011) and Trimmomatic v0.32 (Bolger et al., 2014). Additionally, only reads of 20–25 nucleotides in length and without indeterminations were kept using a custom script. To study the correlation exhibited by the sRNA expression profiles among the different samples, principal component analysis (PCA) was used. PCA was performed using the prcomp function with scaling in the stats R package v. 4.0.4 (R Core Team 2013). Mann–Whitney-Wilcoxon tests were performed to assess for significant differences in the data clusters for Euclidean distances calculated between groups and among groups with the wilcox.test function in the stats R package. Libraries were aligned to the genomes of HSVd (Y09352.1) and *Cucumis sativus* Chinese Long V3 (Zheng et al., 2019) to determine the provenance of every sRNA. Only sequences that aligned with no mismatches exclusively either to the viroid or the plant genome with a minimum of 0.5 RPMs were considered for further analysis. Additionally, for estimating the size abundance, only samples with all the sRNA lengths were considered. Moreover, HSVd-sRNAs were classified according to their origin (positive or negative viroid strand) considering unique sequences and also the accumulation (rpm). Then, an exact binomial test was performed to assess the significance. Differential expression of cucumber sRNAs was estimated using two R packages DESeq. 2 (Love et al., 2014) and edgeR (Robinson et al., 2010) for pairwise differential expression analysis of expression data. Differentially expressed sRNAs were filtered out using two criteria: (i) adjusted $p \leq 0.05$ and (ii) RPMs ≥5 for at least two libraries in stressed or control samples. All p values were adjusted by false discovery rate (FDR). miRNAs were annotated from previously described miRNAs in cucumber (Xu et al., 2020) and validated with the precursors deposited in RNA central (Sweeney et al., 2019). The rest of sRNA categories were annotated using RNA central and sRNAanno (Chen et al., 2021).

2.4 | mRNA sequencing and analysis

RNA sequencing paired reads (150 bp) were aligned to the cucumber genome using STAR (Dobin et al., 2013). For non-annotated transcripts, a de novo assembly was performed using Trinity (Grabherr et al., 2011). A total of 15 589 transcripts non-overlapping with the gene annotation of Chinese Long V3 (Zheng et al., 2019) were aligned with gmap allowing chimeric alignments (Wu & Watanabe, 2005) and a custom annotation of previously unannotated transcripts was obtained using bedtools (Quinlan & Hall, 2010). HTSeq-counts (Anders et al., 2015) was first used to count reads per annotated genes using 10 as a minimum alignment quality and second of the novel annotated transcripts with a minimum alignment quality of 0 and counting all reads ambiguously mapped in both categories and wherever they overlap (to account for potential transposable elements [TEs]). The count tables were used in DESeq. 2 (Love et al., 2014) to infer significant expression, considering an adjusted p value under 0.05 for significance. Clustering analysis of the transcripts with significant differential expression in the three time-points was calculated with stats R-package. First, the optimal number of clusters was determined using the complete method in the NbClust R-package considering Euclidean distances (Charrad et al., 2014). Second, the function '*kmeans*' of stats was applied with one million iterations. The resulting clusters (grouping transcripts with similar evolution of the differential expression profiles over the infection) were generated by ggplot2 (Wickham, 2011). Moreover, to account for differential exon usage, the package DEXSeq was employed (Anders et al., 2012), also considering an adjusted p value under 0.05 for significance. Volcano plots were created using ggplot2 (Wickham, 2011). GO term enrichment analysis was performed using the tool from Cucurbit Genomics Database (CuGenDB) (Zheng et al., 2019). All p values were corrected using FDR and the cutoff p value for significant represented terms was 0.05.

2.5 | Bisulfite sequencing analysis and differentially methylated region (DMR) identification

Whole genome bisulfite sequencing (WGBS) libraries were sequenced by paired end (150 bp). The resulting reads were adapter trimmed and filtered on quality by Trimgalore v0.6.6. Additionally, 10 bases from 5′-ends were trimmed from reads using the same software. The sequence quality was checked by FastQC v0.11.9. The mean conversion rate for the 36 libraries was above 99%. Clean reads were mapped to the reference genome using bismark (Krueger & Andrews, 2011) allowing one mismatch per 25 nucleotides length seed. Alignments at the same position were removed using deduplicate_bismark script, including forward and reverse reads. The bismark_methylation_extractor script was used to extract the methylation call for every single cytosine analyzed and obtain a genome-wide methylation report discriminating by context (CG/CHG/CHH).

The analysis of DMRs was carried out with the R-package DMRcaller (Catoni et al., 2018) dividing the genome in equal bins of 50 bp and pooling the samples of the same condition. The DMR were then computed by performing Fisher's exact test between the number of methylated reads and the total number of reads in both conditions for each bin. The obtained p values were then adjusted for multiple testing using Benjamini-Hochberg's method to control the false discovery (Benjamini & Hochberg, 1995). The criteria chosen to consider a bin as a DMR were the following: (i) adjusted $p \leq 0.05$, (ii) at least three cytosines in the specified context, (iii) more than a 15% methylation difference between the two conditions and (iv) at least an average number of reads of eight. Finally bins that were at less than 300 bp were joined.

In addition to the DMRs identification, overall methylation was calculated as the mean of the percentage methylation of cytosines distinguishing among contexts. Those cytosines covered by less than eight reads were discarded. Next, a heat-map representing the genome-wide methylation difference between the two conditions was performed. First, cytosine methylation percentages were grouped in 3000 nucleotide size windows. Second, the methylation difference was calculated according to time and context. Third, the methylation difference of windows meeting the following terms was set to zero: (i) mock or HSVd show zero reads coverage and (ii) mock and HSVd show less than eight reads coverage. Methylation difference values less than −15% or greater than 15% were considered as −15% and 15%, respectively. Red and blue colours represented the hypomethylation and hypermethylation in HSVd. Both approaches were also carried out for the ribosomal sequence.

3 | RESULTS

3.1 | Viroid infection

To uncover the dynamic of the host response to HSVd we analyzed apical leaves of infected cucumber plants at 10, 17 and 24 dpi. Mock-inoculated plants were used as control. Time points were selected to represent the early, intermediate and late HSVd infection phases (Marquez-Molins et al., 2021). As expected, viroid induced symptoms were evident in HSVd-infected plants at 24 dpi (Figure 1a). A total of 54 libraries (18 for each RNA-seq, small RNA-seq and WGBS) consisting of three biological replicates per time point of infected and control plants were obtained (Figure S1). The information about the number, quality and mapping of the obtained reads for each *-omic* approach is detailed in the Table S1.

The infection rate of inoculated plants was estimated by considering the accumulation of viroid transcripts and vd-sRNAs (Figure 1b,c), recovered from our previously described dataset (Table S1). Viroid transcripts were detected in two (HSVd-R2: 0.53 RPM and HSVd-R3: 46.4 RPM) of the three analyzed samples at 10 dpi, while at 17 dpi an increased number of HSVd transcripts were recovered from all the analyzed samples (132.48, 247.13 and 335.04 RPM for replicates HSVd-R1, HSVd-R2 and HSVd-R3) (Table S2). HSVd-R1 (with no-detected viroid transcripts at 10 dpi) showed an increased accumulation (238.0 RPM) at 24 dpi (Table S2). In contrast, a lower accumulation (in comparison to 17 dpi) of viroid-transcripts was observed in HSVd-R2 (187.3 RPM) and HSVd-R3 (169.4 RPM) samples at 24 dpi. On the other hand, vd-sRNAs were only detected in HSVd-R3 at 10 dpi (1421.0 RPMs). Moreover, and conversely to viroid accumulation in HSVd-R2 and HSVd-R3, sRNAs homologous to HSVd in infected tissues increased through all the analyzed period for the three bio-replicates (Figure 1c and Table S3).

In general, vd-sRNA accumulation correlated ($R = 0.776$, $p = 0.014$) with the accumulation of HSVd transcripts (Figure 1d). HSVd transcripts and vd-sRNAs represented (on average) the 0.002% and 0.047% of the recovered reads at 10 dpi, the 0.024% and 1.5% at 17 dpi and the 0.02% and 2.9% at 24 dpi (Tables S2 and S3). Our results support that both viroid transcripts and vd-sRNAs may be detected in systemic tissues since 10 dpi while already at 17 dpi they reach considerable accumulation levels.

3.2 | Modifications in the host siRNA/miRNA population

Associations between sRNA expression profiles (considering control/infected plants and their biological replicates in the three time points) were evaluated using PCA. The percentage of total variance explained by the first three principal components (PC) was 45.91% and the treatments at the three time points were significantly ($p = 3.05 \times 10^{-12}$) separated in the PC space showing the experimental robustness of the experiment (Figure S2A). The observed accumulation profile of endogenous sRNAs was consistent with previous reports in other cucumber cultivars (Ling et al., 2017; Xu et al., 2019) with a preponderance of 24-nt sRNAs (Figure 2a). However, no significant differences were found between HSVd-infected and control conditions regarding the observed global distribution of sRNAs sizes (two-ways non-parametric analysis of variance, $p = 0.93$; 0.85 and 0.55 for 10, 17 and 24 dpi, respectively).

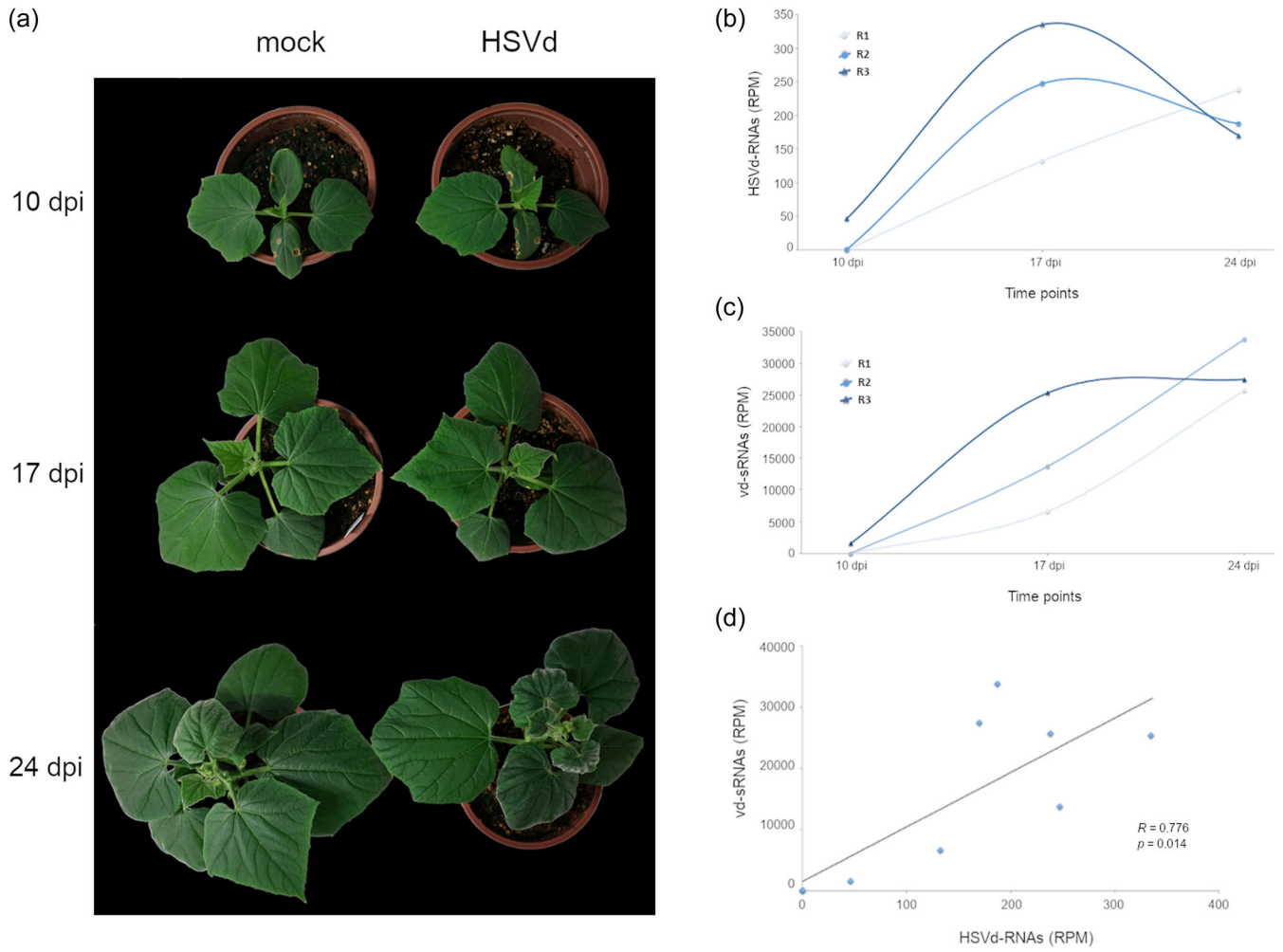

FIGURE 1 HSVd RNA is detected at 10 dpi in infected plants: (a) Representative infected and mock inoculated cucumber plants at the three analyzed time points. Typical plant symptoms characterised by reduction in leaf size and incipient stunting are evident at 24 dpi. Graphic representation of the total transcripts (b) and sRNAs (c) derived from HSVd genome detected in apical leaves at 10, 17 and 24 dpi. (d) Scatter plot showing the significant positive correlation (estimated by Pearson correlation coefficient) between the temporal accumulation of vd-transcript and viroid sRNAs (vd-sRNAs) in infected cucumber plants. dpi, day post inoculation; HSVd, hop stunt viroid. [Color figure can be viewed at wileyonlinelibrary.com]

Only a reduced number (1536 unique reads) of endogenous sRNAs showed significant altered accumulation in HSVd-infected plants at 17 and 24 dpi (no differentially expressed endogenous sRNAs were detected at 10 dpi) (Figure 2b). 145 unique sRNAs were differentially expressed at both 17 and 24 dpi, while 54 and 1337 were only differentially accumulated at 17 or 24 dpi, respectively. A total of 1246 (81.12%) sRNAs were increased in response to the infection, while 290 (18.88%) were decreased. Although no differentially expressed sRNAs were detected at 10 dpi, 199 differential sRNAs (179 overexpressed and 20 downregulated) were identified at 17 dpi (Figure 2c). The most obvious alteration of endogenous sRNA accumulation was observed at 24 dpi with 1482 sequences (1202 upregulated and 280 downregulated) identified as differentially expressed. Overall (considering the differential sRNAs at any time point), 68.42% (1051 unique sequences) of the reactive sRNAs were categorised as derived from ribosomal RNA (rib-sRNAs), while the 7.55% (116 unique sequences) from TEs, and the 3.06% corresponded to 47 unique sequences identified as small interfering RNAs (siRNAs) previously described in cucumber (Figure 2d). A minor representation (1.5%) was observed for known miRNAs, sRNAs derived from snRNAs (1.3%), transfer RNAs (0.52%), small nucleolar RNAs (0.39%) and phased siRNAs (0.2%). The 17.06% of the sRNAs with differential expression were derived from unidentified or not representative functional categories.

We identified seven miRNA families (miR158, miR166, miR171, miR319, miR395, miR397 and miR408) with differential expression associated to HSVd-infection (Figure 2e). Except for miR319 (with 14 unique sequences), the other families were represented by one (miR166, miR171, miR397 and miR408), two (miR395) or three (miR159) differentially expressed unique sequences. All differential miRNAs in each family decreased in response to HSVd-infection (Table S4). miR319 was the only family differentially expressed at

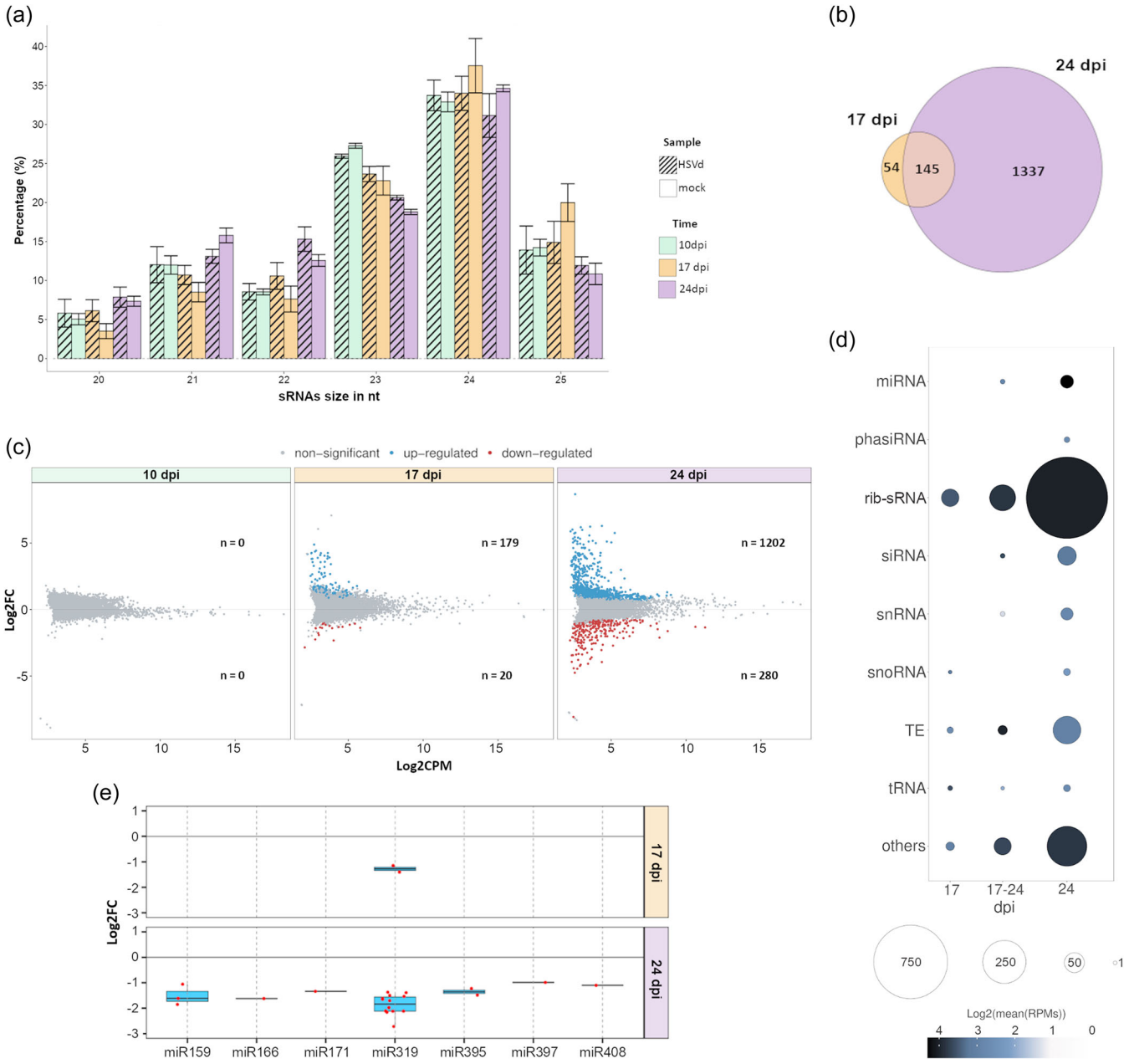

FIGURE 2 Analysis of the sRNA population recovered from the analyzed cucumber libraries. (a) Diagram showing the means of the temporal relative accumulation and distribution of the total sRNAs reads ranging between 20 and 25 nt (error bars indicate the SE between biological replicates). The three analyzed times are represented by colours (green: 10 dpi, orange: 17 dpi and magenta: 24 dpi). Smooth and striped bars represent data arising from mock-inoculated and HSVd-infected plants. (b) Venn diagram representing the number of sRNAs responsive to HSVd infection at 17 and 24 dpi. (c) Volcano plot representing the endogenous cucumber sRNAs with significant differential expression in infected plants at the three analyzed time points. Blue and red dots indicate up- and downregulated sRNAs, respectively. The number of differential sRNAs in each time point is detailed. (d) Categorisation of all the differentially expressed sRNAs in each analyzed time period. The ball size represents the number of unique reads recovered. The colour intensity indicates the sRNA accumulation estimated by the Log2 of the mean of the normalised reads. (e) Box-plot analysis showing the general expression value observed for each miRNA-family member (dots) at 17 and 24 dpi. The differential expression of each miRNA family is represented by the median (internal box line) of the LFC values. dpi, day post inoculation; miRNA, microRNA; phasiRNA, phased secondary small interfering RNA; rRNA, ribosomal RNA; siRNA, small interfering RNA; snRNA, small nuclear RNA; snoRNA, small nucleolar RNA; TE, transposable element; tRNA, transfer RNA. [Color figure can be viewed at wileyonlinelibrary.com]

17 and 24 dpi, the rest of the differential miRNAs were only significant at 24 dpi. The differential expression values of the reactive miRNAs were low (in any case LFC > −1.6), suggesting that the regulatory pathways mediated by miRNAs are not particularly affected by viroid infection.

3.3 | Characterisation of HSVd-derived sRNAs

A total of 1 523 822 reads (representing 7428 unique sequences) fulfilling the conditions (detailed in material and methods) required to be unequivocally considered as HSVd-derived sRNAs (vd-sRNAs) were recovered from the three analyzed time points (Table S2). Analysis of polarity distribution revealed a slight but significant ($p = 2.2 \times 10^{-16}$) difference according to the strand of origin of the vd-sRNAs (58.1% sense and 41.9% antisense) (Figure 3a). This polarity proportion was maintained constant in the three analyzed time points (Figure S3). In contrast, similar proportions for both plus and minus reads were observed when only the number of unique vd-sRNAs was considered (Figure 3b).

Considering each sRNA size-class individually, the sense-strand derived sRNAs were the predominant, except in 20 nt and 23 nt in length vd-sRNAs (Figure 3c). Vd-sRNAs were mainly of 24 nt (68.9%, 57.1% and 49.0% for 10, 17 and 24 dpi, respectively) and 21 nt (15.5%, 24.1% and 30.0% for 10, 17 and 24 dpi, respectively). Except for 22 nt (10.3%, 11.8% and 12% for 10, 17 and 24 dpi, respectively), vd-sRNAs of 20, 23 and 25 nt accumulated less than 5% of the total in the three analyzed time points (Figure 3d). Regarding the predominant vd-sRNAs (24 and 21 nt) the proportion of 21 nt vd-sRNAs increases during viroid-infection while the accumulation of 24 nt reads decreases (two-ways non-parametric analysis of covariance, $p < 0.031$ and 0.039, for 21 and 24 nt, respectively). The observation that a comparable pattern was not detected for endogenous sRNAs (Figure S4), supports that this significant temporal accumulation bias is specific for vd-sRNAs.

If categorised according to their 5′ terminal nucleotide, vd-sRNAs with a C-end were the most abundant (43.8%), followed by reads with T- (24.6%), G- (17.7%) and A- (13.9%) 5'-ends (Figure 3e). A similar distribution of the 5'-end was observed considering size and temporal dynamics of vd-sRNAs (Figure 3f). Furthermore, total vd-sRNAs (recovered at the three time points) were plotted onto HSVd-genome. A heterogeneous distribution pattern could be observed for both sense and antisense vd-sRNAs, in which four obvious hyper accumulation peaks (positions 130 and 254 for the plus and −78 and −184 for the minus polarity the viroid) were detected (Figure 3g). These hyper accumulation peaks predominantly corresponded to 24 nt sRNAs (Figure 3h). The distribution profile of vd-sRNAs was maintained constant during the analyzed infection period (Figure S5). In contrast to hyper accumulation peaks, we observed that a well-defined region of the viroid-genome comprised between the positions 11–38 (plus HSVd polarity) and 31–58 (minus HSVd polarity) showed a null or much lower accumulation of vd-sRNAs in the samples in that vd-sRNAs were detected at three analyzed time points (Figure S6).

3.4 | HSVd-infection modulates the expression and alternative splicing (AS) of host-transcripts

It is expected that the host transcriptome may change in response to the viroid infection. To test that assumption, RNA extracted from control and infected plants was subjected to RNA-seq. Associations between gene expression profiles were evaluated using PCA. The percentage of total variance explained by the first three PC was 62.52% and the treatments/time-points groups were significantly ($p = 1.2 \times 10^{-10}$) separated in the PC space (Figure S2B). A high proportion (98.33%) of the recovered transcript reads in both infected and control plants mapped to the cucumber genome (Table S2), allowing the detection of differentially expressed genes (DEGs) in all time points. The residual reads corresponded to unassigned transcripts (1.66%) and HSVd-derived sequences (0.01%). Considering only reads fully homologous to previously annotated cucumber genes, we identified 1125, 515 and 1390 genes with significant (FDR ≤ 0.05) differential expression in HSVd-infected plants, at 10, 17 and 24 dpi, respectively (Figure 4a and Table S5). A total of 925 (at 10 dpi), 288 (at 17 dpi) and 1052 (at 24 dpi) genes presented time-specific differential accumulation (Figure 4b). Considering a cut-off value of|Log2FC | ≥1, the list of DEGs was reduced to 10 upregulated at 10 dpi, 55 (20 upregulated and 35 downregulated) at 17 dpi and 271 (46 upregulated and 225 downregulated) at 24 dpi (size-increased dots in Figure 4a). The 10 upregulated genes recovered at 10 dpi were only differential at that time point, whereas 27 and 243 genes showed specific differential expression at 17 and 24 dpi, respectively (Figure 4c). Overall, at the first stage of infection (10 dpi), most of the DEGs were upregulated (695 representing 61.7%), whereas downregulation was predominant at 17 dpi (302 genes representing 58.64%) and 24 dpi (975 genes representing 70.14%). A similar trend was observed for genes with (Log2FC ≥ 1 or ≤−1). The amplitude (estimated by the variance of the differential expression values) and diversity (estimated by the number of DEGs) of the transcriptional response to HSVd was clearly increased during the analyzed period of infection (Figure 4d).

According to the analysis of GO-terms, transcriptional response to HSVd-infection was characterised by a significant enrichment in genes associated to diverse biological categories mainly related to metabolic and cellular process, catalytic activity, ribosome metabolism, cellular/intracellular components, transport and membrane (Figure 4e and Table S5). However, the observed number of enriched functional categories at 10 dpi (15 categories) decreased during the infection (6 enriched-categories at 24 dpi). A total of 21 genes were differentially expressed in all the analyzed time points (Figure 4f and Table S6). Except for three genes upregulated in at least one of the analyzed time points (Figure 4g, cluster 2), the common response of the remaining 18 was a stable (cluster 1) or temporally increased (cluster 3) downregulation. These 21 genes were functionally related to transport, membrane activity and response to biotic stimulus. Similarly, a GO-term enrichment analysis of genes more differentially expressed at both 17 and 24 dpi infection phases (considering the threshold |Log2FC | ≥1) revealed the same categories (Figure 4h).

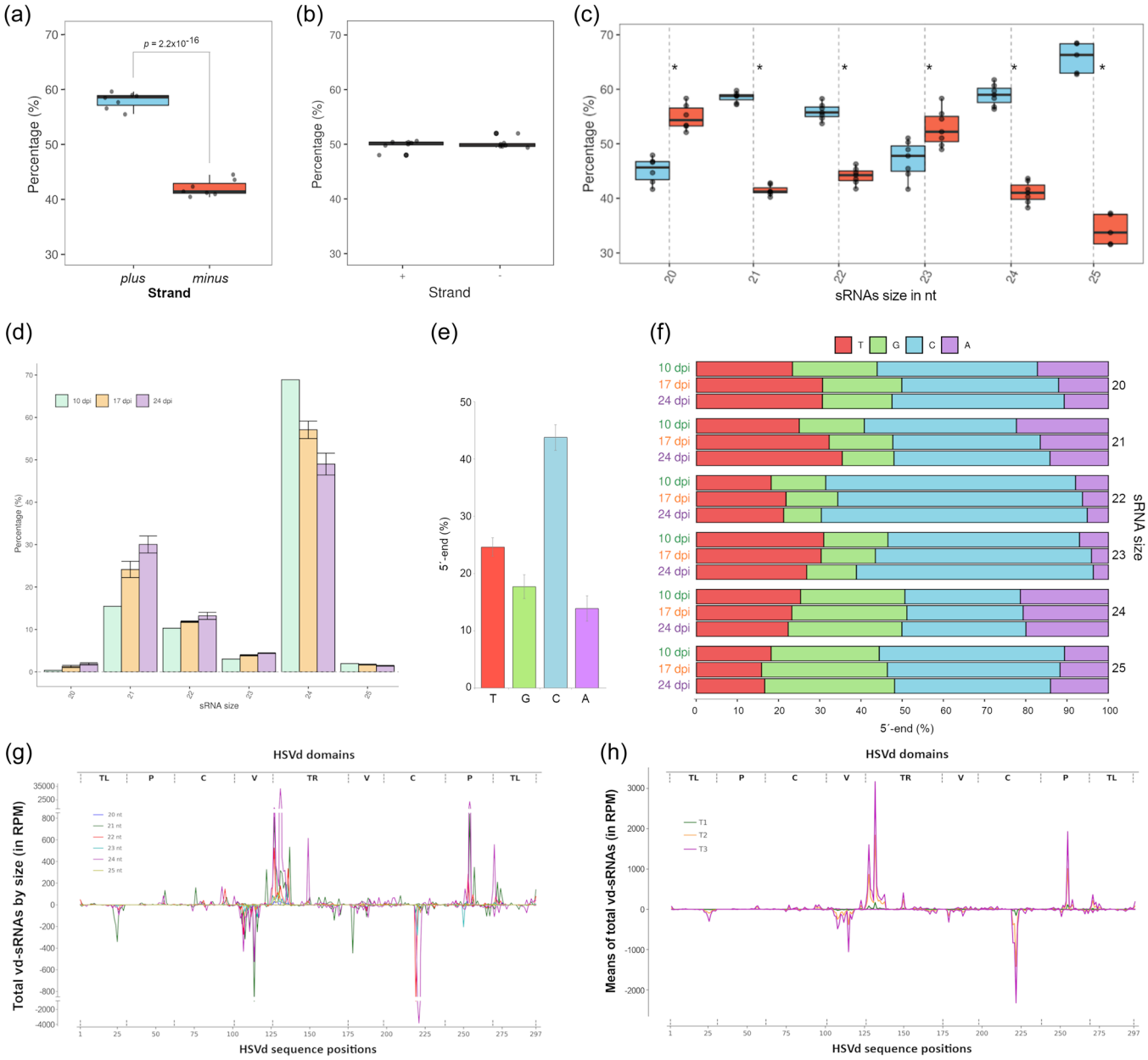

FIGURE 3 Characterisation of vd-sRNAs. (a) Box plot showing the relative accumulation of the total vd-sRNAs (20–25 nt) derived from genomic (plus) and antigenomic (minus) HSVd-RNA strand at the three analyzed time points. (b) Boxplot showing the number of unique reads of vd-sRNAs of each polarity. (c) Polarity distribution of the total vd-sRNAs discriminated by size, asterisks indicate a $p \leq 0.05$ (paired *T*-test). (d) Diagram showing the means of the temporal relative accumulation and distribution of the vd-sRNAs reads ranging between 20 and 25 nts (the error bars indicate the SE, at 10 dpi vd-sRNAs were detected only from one bioreplicate). Colours indicate the three analyzed times (green: 10 dpi, orange: 17 dpi and magenta: 24 dpi). (e) Representation of the proportion of the 5′-ends in the total recovered vd-sRNAs. The means of the total reads are showed. (f) Distribution of the 5′-ends discriminated by size and infection time. (g) Genome view of the vd-sRNAs recovered from infected plants. The vd-sRNAs were plotted according to the position of their 5'-end onto the HSVd-RNA sequence in either sense (above the x-axis) or antisense (below the x-axis) configuration. The values on the y-axis represent the abundance of total vd-sRNAs (sizes indicated by colours) in the three analyzed times. (h) Temporal accumulation of total vd-sRNAs (means of total vd-sRNAs are represented). Vd-sRNAs recovered in each analyzed time are represented by colours (green: 10 dpi, orange: 17 dpi and magenta: 24 dpi). dpi, day post inoculation; miRNA, microRNA; phasiRNA, phased secondary small interfering RNA; rRNA, ribosomal RNA; siRNA, small interfering RNA; snRNA, small nuclear RNA; snoRNA, small nucleolar RNA; TE, transposable element; tRNA, transfer RNA; vd-sRNA, viroid-derived sRNA. [Color figure can be viewed at wileyonlinelibrary.com]

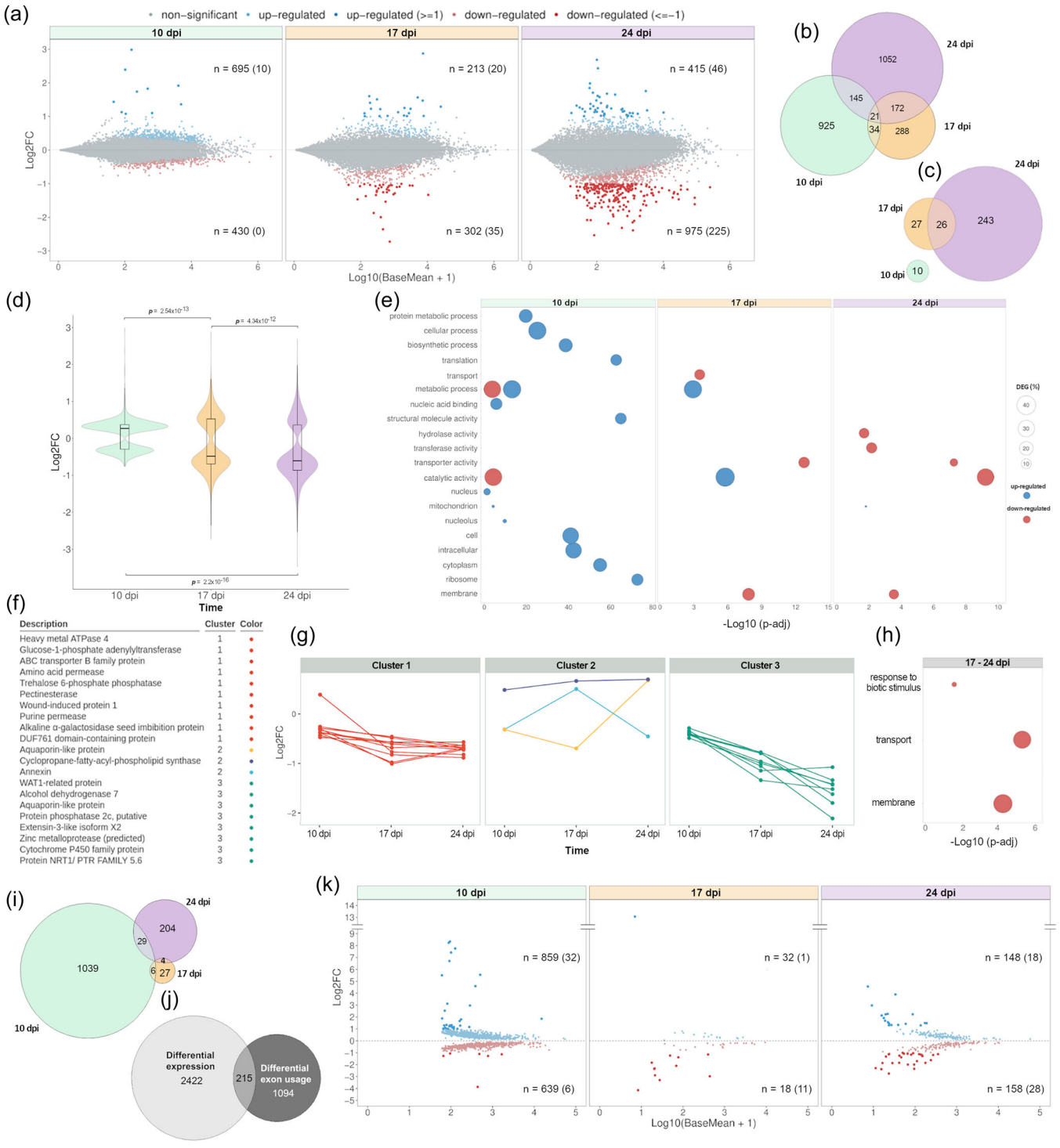

FIGURE 4 Transcriptional alterations associated to HSVd-infection. (a) Volcano plot representing the differentially expressed genes (DEG) in infected cucumber plants at 10, 17 and 24 dpi. Blue and red dots indicate up- and downregulated genes, respectively. DEG with LFC ≥ 1 or ≤−1 are represented by bold dots and the number is indicated in brackets. Venn diagram showing all the DEG (b) and those with LFC ≥ 1 or ≤−1 (c) identified at 10, 17 and 24 dpi. (d) Violin plot representing the temporal profile of the transcriptional alteration associated to HSVd-infection. Internal box line indicates the median of the LFC values. (e) Gene ontology analysis (plant GOSlim) for DEGs identified in HSVd-infected plants at 10, 17 and 24 dpi. Circle size represents the proportion (in percentage) of DEG associated to the GO term (lateral scale). Colour indicates whether the genes are upregulated (blue) or downregulated (red). The −Log(10) of the adjusted *p* values is represented in the x-axis. (f) Detail of the 21 genes differentially expressed in all the three analyzed time-points. Each colour represents a different tendency in the accumulation pattern (g) Clustering analysis of time-course expression profiling of genes with differential expression at 10, 17 and 24 dpi. (h) Gene ontology analysis (plant GOSlim) for genes differentially expressed at both 17 and 24 dpi (LFC ≥ 1 or ≤−1). (i) Venn diagram showing the number of differential exon usage (DEU) events identified at 10, 17 and 24 dpi and (j) genes showing common and specific regulation by differential expression or exon usage. (k) Volcano plot representing the events of DEU in infected plants at 10, 17 and 24 dpi. Blue and red dots indicate up- and downregulated exons, respectively. Events of DEU with LFC ≥ 1 or ≤−1 are represented by bold dots and the number is indicated in brackets. HSVd, hop stunt viroid. [Color figure can be viewed at wileyonlinelibrary.com]

Differential transcripts without previous annotation (and consequently not considered in our study) were analyzed as is described in Section 2 (Figure S7). The obtained results revealed that such transcripts (mainly identified as non-coding-RNAs) exhibited minimal alterations in response to HSVd infection (Table S7).

AS has been proposed as a regulatory mechanism crucial for the modulation of the plant development and response to virus infection (Mandadi & Scholthof, 2015). Sequenced reads were analyzed with DEXSeq tool to infer the AS landscapes of cucumber plants and determine their differential patterns during HSVd infection. We identified 1589 differential exons derived from 1309 intron-containing multiexonic genes that were alternatively spliced in infected plants (Figure 4i). Among such genes, only 215 (5.76%) also showed differential expression (Figure 4j). Furthermore, significant differential exon usage (DEU) was predominantly observed in infected plants at 10 dpi (1498 exons with DEU), less frequent at 24 dpi (306) and a residual phenomenon at 17 dpi (with 50 AS events identified) (Figure 4k and Table S8). Differential exon usage in response to HSVd-infection was comparable at early (38 exons) and late infection phases (46 exons) when we considered only Log2FC values ≥1 or ≤−1 (size increased dots in Figure 3k). Regarding the temporal trend in the differential exons usage, our results support that HSVd infection is associated to a predominant retention of exons at 10 dpi showing 32 over-represented exons with Log2FC values ≥1 (Figure 4k). In contrast, the underrepresented exons (with Log2FC ≥ −1) were prevalent at 17 (11 exons) and 24 dpi (28 exons). Genes exhibiting DEU, at both early (10 dpi) and late (24 dpi) infection phases were predominantly involved in primary metabolism-related process (Figure S8). Additionally, genes associated to membrane and transport, were enriched at 10 dpi.

3.5 | Epigenetic alterations associated to HSVd-infection

To analyze if HSVd-infection modifies the epigenetic landscape of cucumber plants, whole-genome bisulfite sequencing (WGBS) libraries were constructed. Total sequence-coverage obtained from both mock and HSVd-inoculated plants was comparable attesting for the reproducibility of our assays (Figure S9). Global analysis (considering the total percentage of cytosine methylation in CG, CHG and CHH sequence context) revealed a non-significant hypomethylation in infected plants at 10 dpi (70.39% vs. 67.21%, for control and infected plants, respectively), followed by a slight hypermethylation at 17 dpi (75.04% vs. 76.93%) that was significant (70.6% vs. 72.1%) at 24 dpi (Figure 5a, upper panel). These differences were also maintained when the total methylation level for each sequence context was considered (Figure 5a—lower panel). A similar scenario was observed considering each cucumber chromosome individually (Figure 5b). To obtain a more precise picture of the specific methylation changes, we used DMRcaller (Catoni et al., 2018) to identify DMRs for the three CG, CHG, and CHH sequence contexts. Only significant DMRs with differences in methylation ≥15% were considered. The hypomethylated CG DMRs were the most abundant during the analyzed infection period. Conversely, hypermethylated DMRs were more abundant in CHG and CHH sequence contexts (Figure 5c). This global trend was maintained during the three analyzed time points. Considering the intensity (assumed as the median of the DMRs values) in each time and context, the higher values for both hypo (19.4%, 19.8% and 19.5% for 10, 17 and 24 dpi, respectively) and hypermethylation (19.2%, 19.3% and 19.5% for 10, 17 and 24 dpi, respectively) were observed for the CG context. For the DMRs of the CHG context, the medians of the differential methylation were near to the 18% during the entire analyzed period, while for the CHH context the differences were around 17% with no obvious differences between hyper and hypermethylated. Considering the functional categories of the DMRs, approximately 60% of the observed CG DMRs in the three analyzed time points were mapped in regions predicted as coding sequences (CDS) and introns, while intronic regions constituted the predominant DMRs at the CHG context (Figure 5e). As expected, during the analyzed period, CHH DMRs were enriched in TEs and strongly diminished in CDS.

It has been previously demonstrated that HSVd infection promotes alterations in the epigenetic landscape of regulatory regions of the ribosomal DNA (rDNA) (Martinez et al., 2014) to reconfigure a functional scenario that encourages its replication in cucumber plants (Castellano, Pallas, et al., 2016). To extend this study, we analyzed if rDNA was specifically identified as a significant DMR. A region of 150 nt comprised between positions 1984–2133 of the ribosomal genes and overlapping with their promoter region was identified as differentially hypomethylated in CG and CHG contexts at 10 dpi (boxed region in Figure 5f and Figure S10). Moreover, considering the total methylation levels at CG context, HSVd induces a significant ($p = 2.2 \times 10^{-16}$) hypomethylation of the rDNA (79.57% and 77.5% of total methylation for mock and HSVd-infected plants, respectively) at 10 dpi. Although the decrease in the methylation levels was more evident in the promoter region (identified as a significant DMR), the hypomethylated status was extended to the entire ribosomal gene (Figure 5f—upper panel).

Epigenetic alteration of the rDNA associated to HSVd infection was revealed as a dynamic phenomenon, being comparable to mock at 17 dpi (Figure 5f—central panel) and significantly (1.5×10^{-10}) hypermethylated at 24 dpi with total-CG methylation levels of 80.94% and 83.7% for mock and HSVd-infected plants, respectively (Figure 5f—lower panel). This dynamic alteration of the host epigenetic landscape was also observed when CHG and CHH sequence contexts were considered (Figure 5g and Figure S10). Under a temporal viewpoint, the significant hypomethylation of ribosomal genes was coincident with the initial phase in which HSVd reaches a systemic infection, while the transition to an hypermethylation status in host rDNA was in parallel with the stabilisation (or slight decrease) of the HSVd transcripts in infected plants (Figure S11).

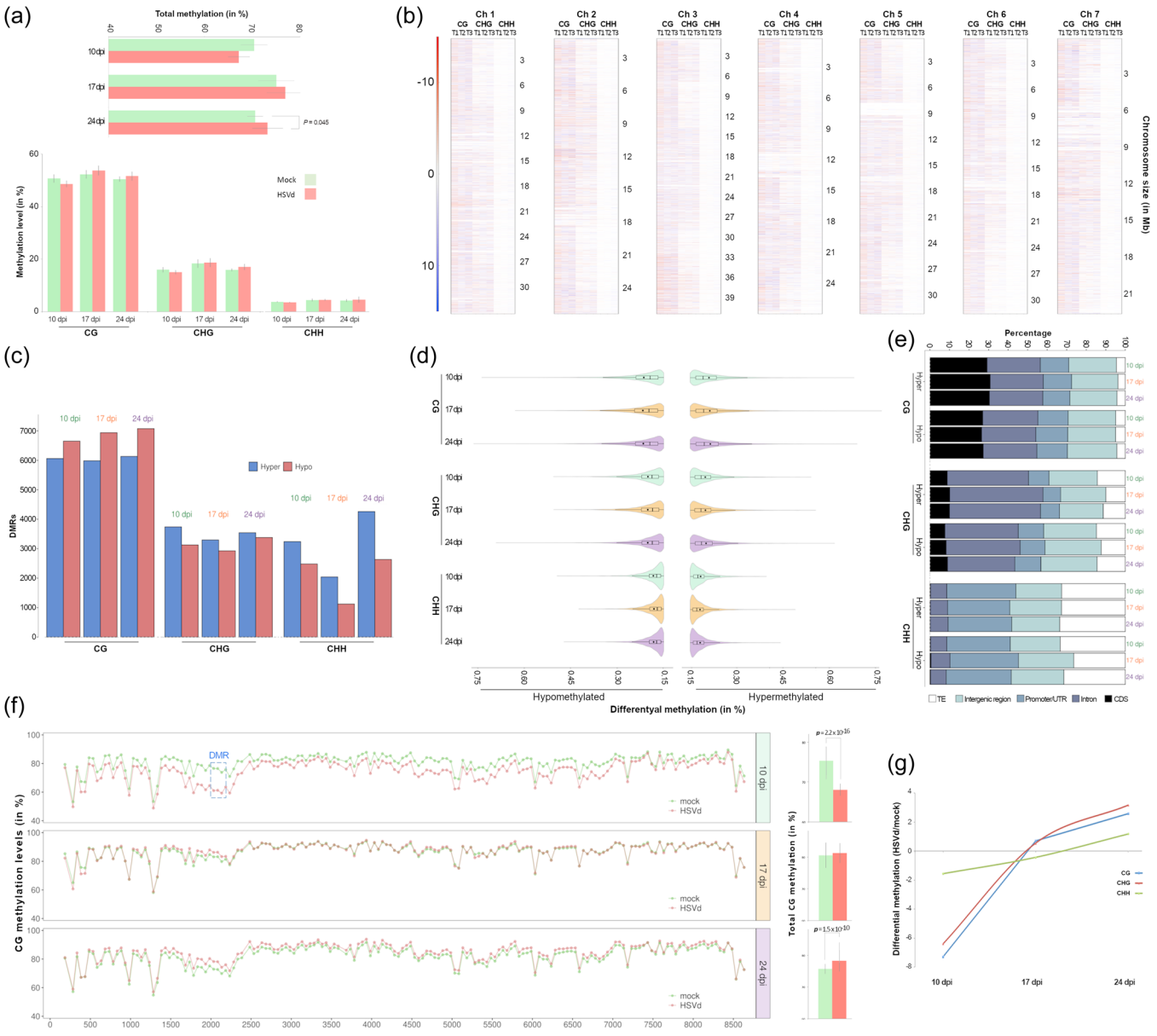

FIGURE 5 HSVd induces alterations in the cucumber epigenetic landscape. (a) Graphic representation of the total cytosine methylation mean values of HSVd-infected and control plants at 10, 17 and 24 dpi (upper panel) and discriminated by sequence context (lower panel). Error bars indicate the standard error between replicates. (b) Chromosome view of the temporal dynamics of the differential methylation profiles in HSVd-infected plants at 10 (green), 17 (orange) and 24 dpi (purple). Red and blue lines represent hypomethylated and hypermethylated regions, respectively. (c) Number of significant hyper- or hypo- differentially methylated regions (DMRs) of more than 15% in the three sequence contexts (CG, CHG and CHH) identified in infected plants at 10, 17 and 24 dpi. (d) Violin plot representing the temporal profile of the epigenetic alterations (estimated by significant DMRs) associated to HSVd-infection. Internal box line indicates the median of the percentage of differential methylation values. (e) Temporal description of the proportion of the cucumber genome regions containing significant DMRs identified in infected plants. (f) Global view of the methylation profiles in CG context in ribosomal RNA transcriptional unit at 10, 17 and 24 dpi in HSVd-infected (red) and control (green) plants. In the left part each dot represents the mean methylation values of 50 nucleotides while in the right the total mean methylation values of the whole ribosomal unit are represented. A significantly hypomethylated DMR identified in infected plants at 10 dpi and matching to promoter region is highlighted. The ribosomal genes (18S, 5.8S and 25S) are indicated in blue while the internal transcribed spacers (ITS) and external transcribed spacers (ETS) are in black. (g) View of the temporal dynamics of the differential methylation in the three sequence contexts (CG, CHG and CHH) observed in ribosomal RNA transcriptional unit during the HSVd infection. dpi, day post inoculation; HSVd, hop stunt viroid. [Color figure can be viewed at wileyonlinelibrary.com]

3.6 | Interplay between methylation and transcriptional regulation in infected plants

To analyze if the changes in the methylation levels observed in HSVd-infected plants could be associated to transcriptional alterations we integrated the data obtained by RNA-seq and WGBS assays. A total of 113 protein-coding genes with strong (Log2FC ≥ 1 or ≤−1) differential expression at 24 dpi containing at least one DMR in any of these regions (promoter/UTR, CDS and intron) were selected for this analysis (Table S9). We observed that 68 of these 113 genes —representing a significant ($p = 0.038$ in Exact binomial test) proportion (60.2%) of the analyzed genes—were characterised by containing at least one DMR with inverse correlation between DNA methylation and gene expression (hypomethylated for upregulated genes or hypermethylated for downregulated genes) (Table S10). Interestingly, a significant negative correlation was observed when we compared their expression levels (estimated by Log2FC) with their global methylation status (determined by DMR analysis in the three sequence contexts) in promoter/UTR and CDS regions ($p = 0.003$ and 0.014, respectively) (Figure 6a). No significant correlation was observed for DMRs matching to introns ($p = 0.148$). A more detailed analysis (focused on each context separately) evidenced that the negative correlation was mainly associated to DMRs in the CG context (Figure 6b and Figure S12). Next, we compared the expression and methylation levels of these 68 genes at 10, 17 and 24 dpi to obtain a global overview of the temporal dynamics of the interplay between cytosine methylation and transcriptional response during HSVd-infection. Our results indicate that while the intensity and the density of the global methylation of the analyzed genes (estimated by the mean values and the total number of the DMRs) were increased during the analyzed period (Figure 6c, upper panel—left), their expression (estimated by the mean of the Log2FC values and the number of DEG) was consistently downregulated (Figure 6c, lower panel—left). In a similar way, the genes upregulated during HSVd-infection were associated to a temporally increased hypomethylation status of their respective genes (Figure 6c, right—lower and upper panel, respectively). According to their biological function, the cucumber genes showing methylation levels antagonistic to transcripts accumulation mainly encoded proteins related to membrane (associated to stress response or transport), oxidation-reduction and metabolic processes (Table S10). Additionally, some genes encoding for nucleus components, transcription factors and protein involved in protein-protein interactions, were also identified.

Regarding the regulation of non-coding transcripts by epigenetic changes, we analyzed the expression of the cucumber ribosomal genes, which has been earlier described to be modulated by HSVd infection (Martinez et al., 2014). Our data showed that the significant hypomethylation of rDNA observed at early infection phases was associated to an increased expression of rRNA genes determined by the increased accumulation of primary precursors of the ribosomal transcripts (pre-rRNAs) in infected plants (Figure S13—left panel). During rRNA transcription, RNA polymerase I transcribes length-units pre-rRNAs that are extensively processed into 18S, 5.8S and 25S units by the sequential deletion of external and internal transcribe spacers (ETS and ITS, respectively) (Henras et al., 2008). Consequently, the differential accumulation of pre-rRNAs was estimated by considering the transcripts matching to ITS1 and ITS2 regions. Finally, the over accumulation in infected plants of rRNA-derived sRNAs (rb-sRNAs), an indirect indicator of the transcriptional activation of normally inoperative rRNA transcriptional units (Earley et al., 2010), provided additional support to the link between rDNA hypomethylation and transcriptional deregulation (Figure S13—right panel).

4 | DISCUSSION

The analysis of the data obtained from high throughput approaches has proved to be valuable to elucidate the regulatory basis of the plant-environment interactions (Depuydt & Vandepoele, 2021; Yang et al., 2021). Therefore, the generation of large-scale datasets constitutes an integral component of modern molecular biology and biotechnology (Jamil et al., 2020).

However, gaining insights through individual *omics* approaches may be insufficient and the integration of these technologies could be an efficient strategy to decipher the biological pathways and regulatory networks underlying the response to stress (including pathogen infection) in plants (Jamil et al., 2020; Zenda et al., 2021). Furthermore, multi-*omics* strategies combined with longitudinal experimental design (considering different time points) can reveal dynamic relationships between *omics* layers and identify key players or regulatory interactions (Bodein et al., 2022). In this sense, the longitudinal integration of multi-*omics* approaches was recently used to provide insights about the temporal transcriptomic and epigenomic reprograming in *Arabidopsis thaliana* plants in response to turnip mosaic virus infection (Corrêa et al., 2020).

As other cellular parasites, viroids are compelled to subvert cellular factors and reprogramme host gene expression to modulate (into their own benefit) complex plant regulatory networks. Assuming this functional scenario, it is expected that the type of affected host-regulatory pathways as well as the intensity of the induced alterations may vary considerably during the infection process. However, our knowledge about the diversity and temporal dynamics of the global plant response to viroid infection is limited (Adkar-Purushothama & Perreault, 2020; Navarro, Flores, et al., 2021).

Here, we have performed a temporal analysis of the global response to HSVd infection focused on three host regulatory levels: RNAi, gene expression and epigenetic modifications. This integrative analysis allowed us to generate a detailed picture, at *omics* scale, of the global host-alterations associated to HSVd infection during the analyzed period. Furthermore, the analysis of the systemic host response at 10 dpi constitutes the earliest infection-stage analyzed at this moment, by any viroid-host interaction (Table S11).

The detection of viroid-derived transcripts and sRNAs in non-inoculated apical tissues at 10 dpi evidenced the capacity of HSVd to

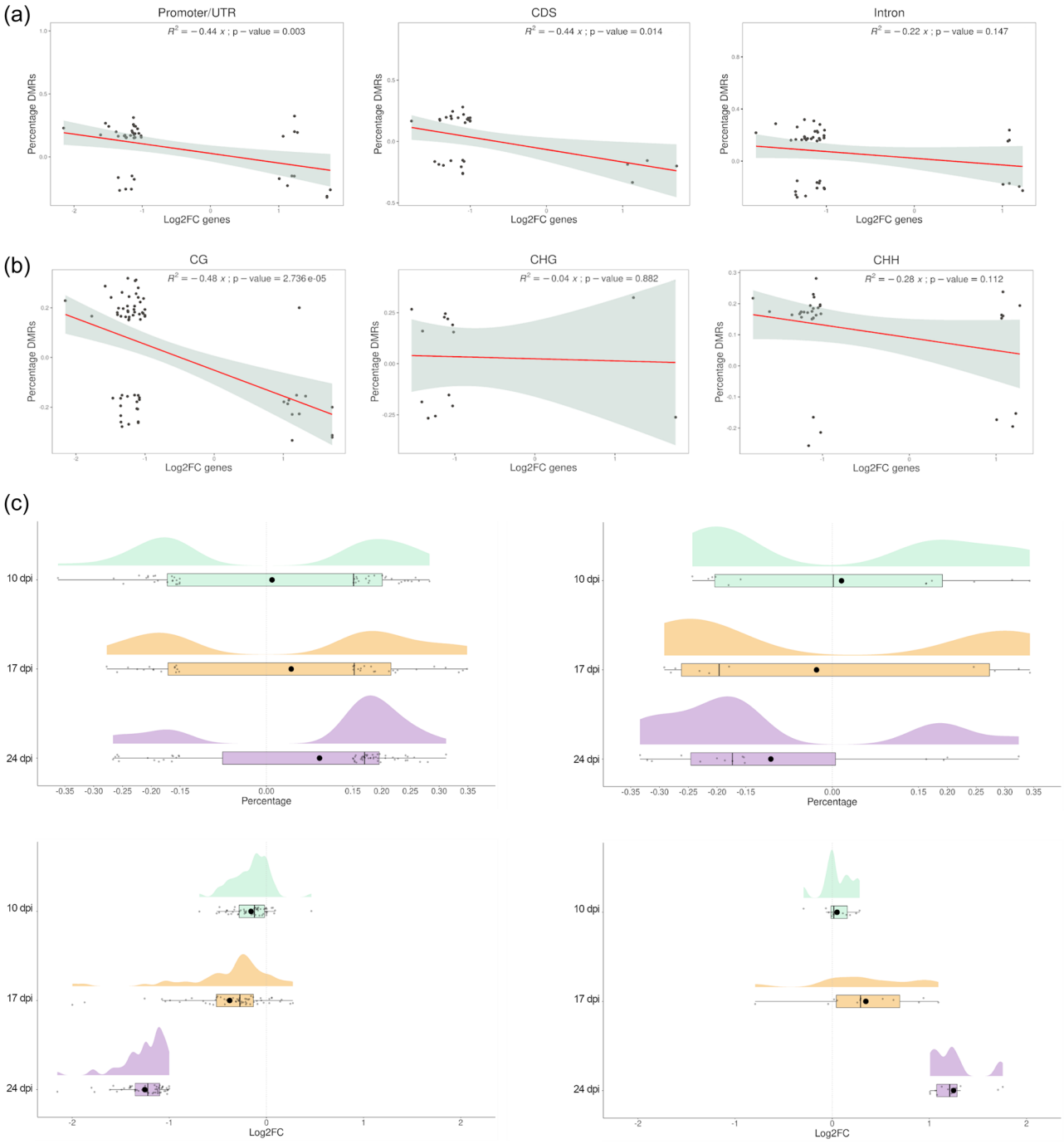

FIGURE 6 Association between transcriptional alterations and epigenetic changes induced by HSVd-infection. Scatter plots showing the negative correlation (significance estimated by Pearson correlation coefficient) between the expression levels of differential genes containing at least one antagonistic DMR and their global methylation status. (a) Considering the three selected gene regions (Promoter/UTR, CDS and intron) and (b) considering methylation sequence context. (c) Raincloud plots showing the temporal correspondence between the sense and the intensity of the epigenetic changes (upper panels) and the gene expression (lower panels) in response to HSVd-infection. The temporal increase in the intensity of the hypermethylated (upper left) and hypomethylated (upper right) DMRs represented by the mean of the differential methylation (black dots) is associated with a decrease (lower right) or increase (lower left), respectively (in intensity) of the gene expression estimated by the LFC mean values (black dots). CDS, coding sequences; DMR, differentially methylated region; HSVd, hop stunt viroid; UTR, untranslated region. [Color figure can be viewed at wileyonlinelibrary.com]

develop a relatively quick systemic infection in cucumber plants. The detection of vd-sRNAs of both *plus* and *minus* polarities at the three analyzed time points, is in accordance with previous studies supporting the predominant involvement of viroid replication intermediates as source of vd-sRNAs (Itaya et al., 2001; Martínez de Alba et al., 2002; Martinez et al., 2010; Navarro et al., 2009; Di Papaefthimiou et al., 2001; Sano & Matsuura, 2004; Di Serio et al., 2009). Considering the size distribution, although vd-sRNAs of 24-nt were the most predominant, the accumulation profile varied during the infection. We observed a temporal increase of the proportion of 21 nt that negatively correlates with the accumulation of 24 nt vd-sRNAs. These results support that the processing/accumulation of 24 nt vd-sRNAs is predominantly associated to initial infection steps, while the accumulation of the 21 nt class constitutes an event characteristic of well-established infectious processes. The observation that a similar scenario is not observed when cucumber sRNAs were considered evidenced the independence of this phenomenon with the natural evolution of the endogenous sRNAs biogenesis. This temporal trend may explain the inconsistency between our data and previous results supporting that 21 nt in length is the most abundant class of vd-sRNA in HSVd-infected cucumber plants at late infection phases (Martinez et al., 2010; Zhang et al., 2020).

Endogenous sRNAs remains relatively stable in response to viroid accumulation, with only 1482 unique sRNAs with significant altered expression at 24 dpi. The predominant trend of this response was the upregulation of the host-derived sRNAs. Differentially expressed sRNAs were not identified at 10 dpi, while a considerable proportion of the sRNAs with significant differential expression observed at 17 and 24 dpi were derived from ribosomal transcripts and associated to hypomethylation of rDNA induced by HSVd-infection. A similar scenario (characterised by a lower reactivity level) was observed when alteration in miRNA population was analyzed. Demonstrating that, in coincidence with the described in other plant-viroid models (Martín et al., 2007; Navarro, Gisel, et al., 2021; Tsushima et al., 2015; Zheng et al., 2017), the weak effects of HSVd infection in the host miRNA profile.

Altered accumulation of plant transcripts, at specific infection phases, has been previously reported in diverse viroid-host interactions (Herranz et al., 2013; Itaya et al., 2002; Owens et al., 2012; Rizza et al., 2012; Zheng et al., 2017). Our temporal analysis of the evolution of the cucumber transcriptional landscape in response to HSVd infection indicates that although significant transcriptional alterations were observed in the three analyzed time points, the intensity of this response paralleled the development of the infection, being slight at 10 dpi and more evident at 24 dpi. Another particularity associated to the infection time was the trend of the transcriptional response, while the upregulation of host genes was the predominant response at 10 dpi, the downregulated genes were predominant at 17 and 24 dpi. According to the functionality, HSVd-infection was associated to an extensive reprogramming of cucumber genes involved in diverse cellular functions. This observation is in agreement with previous data obtained from plants infected with two (severe and mild) HSVd-variants, showing a complex array of changes in the host transcriptome associated to viroid infection (Xia et al., 2017). However, a more defined functional response to HSVd-infection was evident when we considered only genes differentially expressed at 17 and 24 dpi. Cucumber genes included in this common response were predominantly downregulated and mainly involved in membrane metabolism, transport and response to biotic stress.

Besides transcript accumulation, it is well established that AS is a regulated process that increases the transcriptome diversity, providing an alternative way to favour the plant adaptation to environmental changes (Jabre et al., 2019; Shang et al., 2017). However, our knowledge about the alternative processing of host transcripts in response to viroid infection is very limited and only data related to PSTVd-infected tomato plants at late infection has been reported (Zheng et al., 2017). Our results evidenced that the differential exon usage was the predominant transcriptional response during the initial phase of the HSVd-infection (10 dpi). In contrast to the observed for gene expression, the global trend (up or downregulation) in exon accumulation was comparable at the three analyzed time points. Only a small proportion (5.76%) of the genes having AS, also exhibited significant differential expression, suggesting that the control of the transcriptional activity and the alternative processing of pre-mRNAs might be complementary mechanisms activated in cucumber plants in response to HSVd infection. Regarding to the functionality of the transcripts with significant DEU in response to HSVd-infection, we observed that although the initial response included genes involved in many cellular processes, transcripts showing a relatively constant DEU frequency during infection, were predominantly related to primary metabolism. The observation that AS of transcripts with similar biological functions was also reported in PSTVd-infected tomato plants (Zheng et al., 2017), suggest that the regulation of the plant metabolism mediated by DEU might be a host response mechanism also extended to other nuclear-replicating viroids.

The differential methylation of cytosines is another host regulatory layer susceptible to be affected in response to viroid infection (Wassenegger & Dalakouras, 2021). Although, this epigenetic mechanism was first described studying viroid infection in PSTVd-expressing transgenic tobacco plants (Wassenegger et al., 1994), the global effects of viroid-infection into host DNA methylation, remain yet unexplored (Navarro, Flores, et al., 2021). The WGBS analysis evidenced that HSVd infection is associated with significant alterations in the host epigenetic landscape. Under a global viewpoint, the alteration in cytosine methylation was a dynamic phenomenon associated to infection phases and sequence context. Studying in detail the regulatory effects of this altered epigenetic landscape; we observed that the changes in methylation levels (at CG sequence context) of putative promoter regions and CDS correlate with the transcriptional alterations observed in infected plants. Thus, suggesting that these HSVd-associated epigenetic variations may be responsible of the differential expression of certain genes in infected cucumber plants.

The integrative analysis of our data supports that in response to HSVd significant alterations are triggered in cucumber plants at

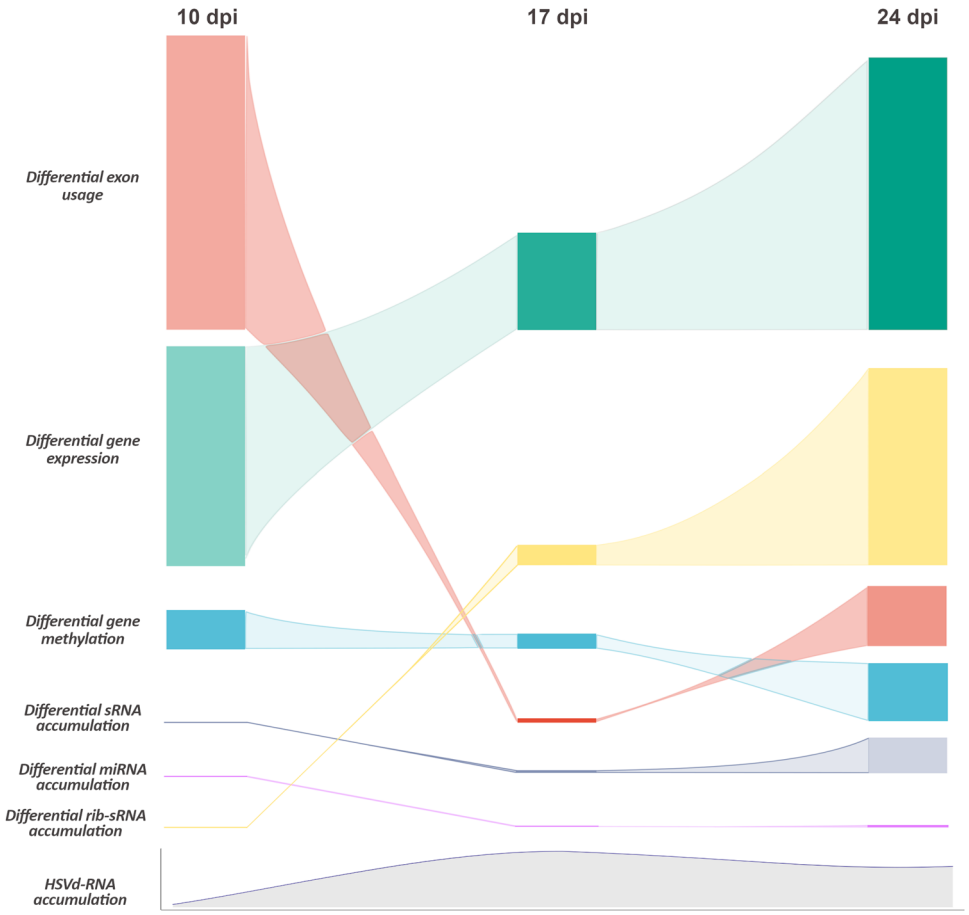

FIGURE 7 Graphic representation showing the temporal dynamics of the global host-regulatory response to HSVd-infection in cucumber plants. The predominant regulatory layers affected in each analyzed infection time are hierarchical represented by the density (box length) estimated by the number of alterations and intensity (box colour strength) estimated by the absolute differential value of the response. To represent the density of the alterations in methylation we considered the number of genes with significant DMRs in CG context. In the sRNA group are included all the identified classes except the derived from ribosomal RNA (rib-sRNAs) and miRNAs. The global position in each analyzed time-point indicates the predominance of the regulatory layer in the global response to infection. Below it is also represented the relative accumulation of HSVd estimated by the number (in RPM) of viroid transcripts recovered from infected plants. DMR, differentially methylated region; HSVd, hop stunt viroid; miRNA, microRNA. [Color figure can be viewed at wileyonlinelibrary.com]

different regulatory levels that are closely related to the temporal dynamics of the infection process (Figure 7). Differential exon usage, modulated by AS, emerges as the predominant response at the initial infection stage. It is well established that the alternative processing of the pre-mRNAs increases the diversity of the plant transcriptome and proteome (Shang et al., 2017). Consequently, this rearrangement of the host-transcriptome (without new transcriptional activity) might, in similar way to the previously described for other stress conditions (Jabre et al., 2019), allow the immediate fine tuning of the host gene expression in response to HSVd-infection. At subsequent infection phases, the modulation of the plant-response to the viroid would be mainly promoted by alterations in the gene expression, which was increased at 17 dpi and being the mostly affected regulatory-layer (considering both, intensity and diversity) at 24 dpi. Interestingly, altered transcription shows a temporal coincidence with changes in the methylation profiles of promoter regions in certain cucumber genes. This functional connection permits to speculate about the possibility that the non-immediate transcriptional response to HSVd might be modulated by the host epigenetic changes associated to infection. Finally, it was obvious that the alteration in sRNA and miRNA metabolism played a minor functional role in the recovering of the cell homeostasis in response to HSVd infection.

In conclusion, the comprehensive *multi-omics* approach reported here constitutes the most complete dataset currently available about the global and temporal host response to viroid infection. Recognising that this is only the initial step in a long road, we expect that this extensive dataset will constitute a valuable framework for future research focused on understanding the mechanistic and the molecular basis of the host changes triggered in response to viroid infection.

ACKNOWLEDGEMENTS

The authors thank Dr. Beatriz Navarro for critically reading this manuscript. This work was supported by the Agencia Estatal de Investigacion (AEI) (co-supported by FEDER) Grants

PID2019-104126RB-I00 (GG) and PID2020-115571RB-I00 (VP). J.M.M. and J.C.S. was/is recipient of a pre-doctoral contract ACIF-2017-114 and CIACIF-2021-279 from the Generalitat Valenciana. The funders had no role in the experiment design, data analysis, decision to publish, or preparation of the manuscript.

CONFLICT OF INTEREST STATEMENT

The authors declare no conflicts interest.

DATA AVAILABILITY STATEMENT

The data that support the findings of this study are openly available in Sequence Read Archive (SRA) data at https://www.ncbi.nlm.nih.gov/sra, reference number BioProject ID: PRJNA795883.

Sequence datasets used in this study have been uploaded in NCBI SRA under the accession code BioProject ID: PRJNA795883. All the necessary components, including scripts for analysis, annotations, software versions, and additional files required to replicate the study′s findings, as well as Supporting Information Tables with analysis results, can be found on our GitHub page (https://github.com/ncRNA-lab/Cucumber-HSVd).

ORCID

Gustavo Gomez http://orcid.org/0000-0003-3715-7792

REFERENCES

Adkar-Purushothama, C.R. & Perreault, J.-P. (2020) Current overview on viroid–host interactions. *WIREs RNA*, 11, e1570. Available from: https://doi.org/10.1002/wrna.1570

Anders, S., Pyl, P.T. & Huber, W. (2015) HTSeq-A Python framework to work with high-throughput sequencing data. *Bioinformatics*, 31, 166–169.

Anders, S., Reyes, A. & Huber, W. (2012) Detecting differential usage of exons from RNA-seq data. *Genome Research*, 22, 2008–2017.

Annacondia, M.L., Magerøy, M.H. & Martinez, G. (2018) Stress response regulation by epigenetic mechanisms: changing of the guards. *Physiologia Plantarum*, 162, 239–250.

Aviña-Padilla, K., Rivera-Bustamante, R., Kovalskaya, N. & Hammond, R. (2018) Pospiviroid infection of tomato regulates the expression of genes involved in flower and fruit development. *Viruses*, 10, 516. Available from: http://www.mdpi.com/1999-4915/10/10/516 [Accessed November 19, 2021].

Aviña-Padilla, K., Zambada-Moreno, O., Herrera-Oropeza, G.E., Jimenez-Limas, M.A., Abrahamian, P., Hammond, R.W. et al. (2022) Insights into the transcriptional reprogramming in tomato response to PSTVd variants using network approaches. *International Journal of Molecular Sciences*, 23, 5983.

Baulcombe, D.C. & Dean, C. (2014) Epigenetic regulation in plant responses to the environment. *Cold Spring Harbor Perspectives in Biology*, 6, a019471. Available from: https://pubmed.ncbi.nlm.nih.gov/25183832

Benjamini, Y. & Hochberg, Y. (1995) Controlling the false discovery rate: a practical and powerful approach to multiple testing. *Journal of the Royal Statistical Society: Series B (Methodological)*, 57, 289–300.

Bodein, A., Scott-Boyer, M.-P., Perin, O., Lê Cao, K.-A. & Droit, A. (2022) Interpretation of network-based integration from multi-omics longitudinal data. *Nucleic Acids Research*, 50, e27. Available from: https://www.scopus.com/inward/record.uri?eid=2-s2.0

Bolger, A.M., Lohse, M. & Usadel, B. (2014) Trimmomatic: a flexible trimmer for Illumina sequence data. *Bioinformatics*, 30, 2114–2120.

Castellano, M., Martinez, G., Marques, M.C., Moreno-Romero, J., Köhler, C., Pallas, V. et al. (2016) Changes in the DNA methylation pattern of the host male gametophyte of viroid-infected cucumber plants. *Journal of Experimental Botany*, 67, 5857–5868.

Castellano, M., Pallas, V. & Gomez, G. (2016) A pathogenic long noncoding RNA redesigns the epigenetic landscape of the infected cells by subverting host histone deacetylase 6 activity. *New Phytologist*, 211, 1311–1322.

Catoni, M., Tsang, J.M., Greco, A.P. & Zabet, N.R. (2018) DMRcaller: a versatile R/Bioconductor package for detection and visualization of differentially methylated regions in CpG and non-CpG contexts. *Nucleic Acids Research*, 46(19), 992.

Charrad, M., Ghazzali, N., Boiteau, V. & Niknafs, A. (2014) Nbclust: an R package for determining the relevant number of clusters in a data set. *Journal of Statistical Software*, 61, 1–36.

Chen, C., Li, J., Feng, J., Liu, B., Feng, L., Yu, X. et al. (2021) sRNAanno—a database repository of uniformly annotated small RNAs in plants. *Horticulture Research*, 8, 45.

Corrêa, R.L., Sanz-Carbonell, A., Kogej, Z., Müller, S.Y., Ambrós, S., López-Gomollón, S. et al. (2020) Viral fitness determines the magnitude of transcriptomic and epigenomic reprogramming of defense responses in plants. *Molecular Biology and Evolution*, 37, 1866–1881. Available from: https://doi.org/10.1093/molbev/msaa091/5817319

Deleris, A., Halter, T. & Navarro, L. (2016) DNA methylation and demethylation in plant immunity. *Annual Review of Phytopathology*, 54, 579–603. Available from: https://doi.org/10.1146/annurev-phyto-080615-100308

Depuydt, T. & Vandepoele, K. (2021) Multi-omics network-based functional annotation of unknown arabidopsis genes. *The Plant Journal*, 108, 1193–1212. Available from: https://doi.org/10.1111/tpj.15507

Diermann, N., Matoušek, J., Junge, M., Riesner, D. & Steger, G. (2010) Characterization of plant miRNAs and small RNAs derived from potato spindle tuber viroid (PSTVd) in infected tomato. *Biological Chemistry*, 391, 1379–1390. Available from: https://doi.org/10.1515/bc.2010.148

Ding, B. (2009) The biology of viroid-host interactions. *Annual Review of Phytopathology*, 47, 105–131.

Dobin, A., Davis, C.A., Schlesinger, F., Drenkow, J., Zaleski, C., Jha, S. et al. (2013) *Bioinformatics*, 29. STAR: ultrafast universal RNA-seq aligner. pp. 15–21

Earley, K.W., Pontvianne, F., Wierzbicki, A.T., Blevins, T., Tucker, S., Costa-Nunes, P. et al. (2010) Mechanisms of HDA6-mediated rRNA gene silencing: suppression of intergenic Pol II transcription and differential effects on maintenance versus siRNA-directed cytosine methylation. *Genes & Development*, 24, 1119–1132.

Elena, S., Gómez, G. & Daròs, J.A. (2009) Evolutionary constraints to viroid evolution. *Viruses*, 1, 241–254.

Gago-Zachert, S. (2016) Viroids, infectious long non-coding RNAs with autonomous replication. *Virus Research*, 212, 12–24. Available from: https://www.sciencedirect.com/science/article/pii/S0168170215300502

Gómez, G. & Pallás, V. (2001) Identification of an in vitro ribonucleoprotein complex between a viroid RNA and a phloem protein from cucumber plants. *Molecular Plant-Microbe Interactions®*, 14, 910–913.

Gómez, G. & Pallás, V. (2007) Mature monomeric forms of Hop stunt viroid resist RNA silencing in transgenic plants. *The Plant Journal*, 51, 1041–1049.

Gómez, G. & Pallás, V. (2013) Viroids: a light in the darkness of the lncRNA-directed regulatory networks in plants. *New Phytologist*, 198, 10–15.

Gómez-Díaz, E., Jordà, M., Peinado, M.A. & Rivero, A. (2012) Epigenetics of host–pathogen interactions: the road ahead and the road behind C. E. Chitnis, ed. *PLoS Pathogens*, 8, e1003007.

Góra-Sochacka, A., Więsyk, A., Fogtman, A., Lirski, M. & Zagórski-Ostoja, W. (2019) Root transcriptomic analysis reveals global changes induced by systemic infection of *Solanum lycopersicum* with mild and severe variants of potato spindle tuber viroid. *Viruses*, 11, 992.

Gómez, G. & Pallás, V. (2004) A long-distance translocatable phloem protein from cucumber forms a ribonucleoprotein complex in vivo with Hop stunt viroid RNA. *Journal of Virology*, 78, 10104–10110.

Grabherr, M.G., Haas, B.J. & Yassour, M. (2011) *Nat. Biotechnol*, 29. Trinity: reconstructing a full-length transcriptome without a genome from RNA-Seq data, p. 644.

Hadjieva, N., Ivanova, D.P., Yahubyan, G. & Baev, V. (2021) MicroRNA expression dynamics reshape the cultivar-specific response of pepper (*Capsicum annuum* L.) to potato spindle tuber viroid (PSTVd) infection. *Sci. Hortic*, 278, 109845.

Healey, A., Furtado, A., Cooper, T. & Henry, R.J. (2014) Protocol: a simple method for extracting next-generation sequencing quality genomic DNA from recalcitrant plant species. *Plant Methods*, 10, 21.

Henras, A.K., Soudet, J., Gérus, M., Lebaron, S., Caizergues-Ferrer, M., Mougin, A. et al. (2008) The post-transcriptional steps of eukaryotic ribosome biogenesis. *Cellular and Molecular Life Sciences*, 65, 2334–2359. Available from: https://doi.org/10.1007/s00018-008-8027-0

Herranz, M.C., Niehl, A., Rosales, M., Fiore, N., Zamorano, A., Granell, A. et al. (2013) A remarkable synergistic effect at the transcriptomic level in peach fruits doubly infected by prunus necrotic ringspot virus and peach latent mosaic viroid. *Virology Journal*, 10, 164. Available from: https://doi.org/10.1186/1743-422X-10-164

Itaya, A., Folimonov, A., Matsuda, Y., Nelson, R.S. & Ding, B. (2001) Potato spindle tuber viroid as inducer of RNA silencing in infected tomato. *Molecular Plant-Microbe Interactions®*, 14, 1332–1334.

Itaya, A., Matsuda, Y., Gonzales, R.A., Nelson, R.S. & Ding, B. (2002) Potato spindle tuber viroid strains of different pathogenicity induces and suppresses expression of common and unique genes in infected tomato. *Molecular Plant-Microbe Interactions®*, 15, 990–999. Available from: https://doi.org/10.1094/MPMI.2002.15.10.990

Itaya, A., Zhong, X., Bundschuh, R., Qi, Y., Wang, Y., Takeda, R. et al. (2007) A structured viroid RNA serves as a substrate for dicer-like cleavage to produce biologically active small RNAs but is resistant to RNA-Induced silencing complex-mediated degradation. *Journal of Virology*, 81, 2980–2994.

Jabre, I., Reddy, A.S.N., Kalyna, M., Chaudhary, S., Khokhar, W., Byrne, L.J. et al. (2019) Does co-transcriptional regulation of alternative splicing mediate plant stress responses? *Nucleic Acids Research*, 47, 2716–2726. Available from: https://pubmed.ncbi.nlm.nih.gov/30793202

Jamil, I.N., Remali, J., Azizan, K.A., Nor Muhammad, N.A., Arita, M. & Goh, H.-H. et al. (2020) Systematic multi-omics integration (MOI) approach in plant systems biology. *Frontiers in Plant Science*, 11, 944. Available from: https://doi.org/10.3389/fpls.2020.00944

Kappagantu, M., Bullock, J.M., Nelson, M.E. & Eastwell, K.C. (2017) Hop stunt viroid: effect on host (*Humulus lupulus*) transcriptome and its interactions with hop powdery mildew (Podospheara macularis). *Molecular Plant-Microbe Interactions®*, 30, 842–851.

Katsarou, K., Wu, Y., Zhang, R., Bonar, N., Morris, J. & Hedley, P.E. et al. (2016) Insight on genes affecting tuber development in potato upon potato spindle tuber viroid (PSTVd) infection. *PLoS One*, 11, e0150711. Available from: https://pubmed.ncbi.nlm.nih.gov/26937634

Krueger, F. & Andrews, S.R. (2011) Bismark: a flexible aligner and methylation caller for Bisulfite-Seq applications. *Bioinformatics*, 27, 1571–1572.

Lavagi-Craddock, I., Bodaghi, S. & Vidalakis, G. (2021) Next-generation sequencing identification and characterization of microRNAs in dwarfed citrus trees infected with citrus dwarfing viroid in high-density plantings. *Frontiers in Microbiology*, 12, 646273.

Ling, J., Luo, Z., Liu, F., Mao, Z., Yang, Y. & Xie, B. (2017) Genome-wide analysis of microRNA targeting impacted by SNPs in cucumber genome. *BMC Genomics*, 18, 275. Available from: https://doi.org/10.1186/s12864-017-3665-y

Love, M.I., Huber, W. & Anders, S. (2014) Moderated estimation of fold change and dispersion for RNA-seq data with DESeq. 2. *Genome Biology*, 15, 550. Available from: https://doi.org/10.1186/s13059-014-0550-8

Lv, D.Q., Liu, S.W., Zhao, J.H., Zhou, B.J., Wang, S.P., Guo, H.S. et al. (2016) Replication of a pathogenic non-coding RNA increases DNA methylation in plants associated with a bromodomain-containing viroid-binding protein. *Scientific Reports*, 6, 35751.

Mandadi, K.K. & Scholthof, K.-B.G. (2015) Genome-wide analysis of alternative splicing landscapes modulated during plant-virus interactions in *Brachypodium distachyon*. *The Plant Cell*, 27, 71–85. Available from: https://pubmed.ncbi.nlm.nih.gov/25634987

Marquez-Molins, J., Navarro, J.A., Pallas, V. & Gomez, G. (2019) Highly efficient construction of infectious viroid-derived clones. *Plant Methods*, 15, 87. Available from: https://doi.org/10.1186/s13007-019-0470-4

Marquez-Molins, J., Gomez, G. & Pallas, V. (2021) Hop stunt viroid: a polyphagous pathogenic RNA that has shed light on viroid–host interactions. *Molecular Plant Pathology*, 22, 153–162. Available from: https://doi.org/10.1111/mpp.13022

Martin, M. (2011) Cutadapt removes adapter sequences from high-throughput sequencing reads. *EMBnet.journal*, *Vol* 17, 10. *No 1 Next Gener. Seq. Data Anal* https://doi.org/10.14806/ej.17.1.200. Available from: https://journal.embnet.org/index.php/embnetjournal/article/view/200/479

Martín, R., Arenas, C., Daròs, J.-A., Covarrubias, A., Reyes, J.L. & Chua, N.-H. (2007) Characterization of small RNAs derived from citrus exocortis viroid (CEVd) in infected tomato plants. *Virology*, 367, 135–146. Available from: https://www.sciencedirect.com/science/article/pii/S0042682207003510

Martinez, G., Castellano, M., Tortosa, M., Pallas, V. & Gomez, G. (2014) A pathogenic non-coding RNA induces changes in dynamic DNA methylation of ribosomal RNA genes in host plants. *Nucleic Acids Research*, 42, 1553–1562.

Martinez, G., Donaire, L., Llave, C., Pallas, V. & Gomez, G. (2010) High-throughput sequencing of Hop stunt viroid-derived small RNAs from cucumber leaves and phloem. *Molecular Plant Pathology*, 11, 347–359.

Martínez de Alba, A.E., Flores, R. & Hernández, C. (2002) Two chloroplastic viroids induce the accumulation of small RNAs associated with posttranscriptional gene silencing. *Journal of Virology*, 76, 13094–13096.

Navarro, B., Flores, R. & Di Serio, F. (2021) Advances in viroid-host interactions. *Annual Review of Virology*, 8, 305–325. Available from: https://doi.org/10.1146/annurev-virology-091919-092331

Navarro, B., Gisel, A., Serra, P., Chiumenti, M., Di Serio, F. & Flores, R. (2021) Degradome analysis of tomato and nicotiana benthamiana plants infected with potato spindle tuber viroid. *International Journal of Molecular Sciences*, 22, 3725.

Navarro, B., Pantaleo, V., Gisel, A., Moxon, S., Dalmay, T., Bisztray, G. et al. (2009) Deep sequencing of viroid-derived small RNAs from grapevine provides new insights on the role of RNA silencing in plant-viroid interaction. *PLoS One*, 4, e7686.

Owens, R.A., Tech, K.B., Shao, J.Y., Sano, T. & Baker, C.J. (2012) Global analysis of tomato gene expression during potato spindle tuber viroid infection reveals a complex array of changes affecting hormone signaling. *Molecular Plant-Microbe Interactions®*, 25, 582–598.

Papaefthimiou, I. (2001) Replicating potato spindle tuber viroid RNA is accompanied by short RNA fragments that are characteristic of

post-transcriptional gene silencing. *Nucleic Acids Research*, 29, 2395–2400.

Quinlan, A.R. & Hall, I.M. (2010) BEDTools: a flexible suite of utilities for comparing genomic features. *Bioinformatics*, 26, 841–842.

Rizza, S., Conesa, A., Juarez, J., Catara, A., Navarro, L., Duran-Vila, N. et al. (2012) Microarray analysis of Etrog citron (*Citrus medica* L.) reveals changes in chloroplast, cell wall, peroxidase and symporter activities in response to viroid infection: genomic survey of viroid infection in early stages. *Molecular Plant Pathology*, 13, 852–864. Available from: https://doi.org/10.1111/j.1364-3703.2012.00794.x

Robinson, M.D., McCarthy, D.J. & Smyth, G.K. (2010) edgeR: a bioconductor package for differential expression analysis of digital gene expression data. *Bioinformatics*, 26, 139–140.

Sano, T. & Matsuura, Y. (2004) Accumulation of short interfering RNAs characteristic of RNA silencing precedes recovery of tomato plants from severe symptoms of potato spindle tuber viroid infection. *Journal of General Plant Pathology*, 70, 50–53. Available from: https://doi.org/10.1007/s10327-003-0083-6

Sanz-Carbonell, A., Marques, M.C., Bustamante, A., Fares, M.A., Rodrigo, G. & Gomez, G. (2019) Inferring the regulatory network of the miRNA-mediated response to biotic and abiotic stress in melon. *BMC Plant Biology*, 19, 78.

Sanz-Carbonell, A., Marques, M.C., Martinez, G. & Gomez, G. (2020) Dynamic architecture and regulatory implications of the miRNA network underlying the response to stress in melon. *RNA Biology*, 17, 292–308.

Di Serio, F., Li, S.-F., Pallás, V., Owens, R.A., Randles, J.W., Sano, T. et al. (2017) In: Hadidi, A., Flores, R., Randles, J.W., Palukaitis, P., eds. *Chapter 13 - Viroid Taxonomy*. Boston: Academic Press. pp. 135–146. Available from: http://www.sciencedirect.com/science/article/pii/B9780128014981000139

Di Serio, F., Gisel, A., Navarro, B., Delgado, S., Martínez de Alba, Á.E., Donvito, G. et al. (2009) Deep sequencing of the small RNAs derived from two symptomatic variants of a chloroplastic viroid: implications for their genesis and for pathogenesis. *PLoS One*, 4, e7539. Available from: https://pubmed.ncbi.nlm.nih.gov/19847296

Di Serio, F., Owens, R.A., Navarro, B., Serra, P., Martínez de Alba, Á.E., Delgado, S. et al. (2023) Role of RNA silencing in plant-viroid interactions and in viroid pathogenesis. *Virus Research*, 323, 198964. Available from: https://www.sciencedirect.com/science/article/pii/S0168170222002933

Sečnik, A., Štajner, N., Radišek, S., Kunej, U., Križman, M. & Jakše, J. (2022) Cytosine methylation in genomic DNA and characterization of DNA methylases and demethylases and their expression profiles in viroid-infected Hop plants (*Humulus lupulus* Var.'Celeia'). *Cells*, 11, 2592. Available from: https://pubmed.ncbi.nlm.nih.gov/36010668

Shang, X., Cao, Y. & Ma, L. (2017) Alternative splicing in plant genes: a means of regulating the environmental fitness of plants. *International Journal of Molecular Sciences*, 18, 432. Available from: https://pubmed.ncbi.nlm.nih.gov/28230724

Sweeney, B.A., Petrov, A.I., Burkov, B., Finn, R.D., Bateman, A., Szymanski, M. et al. (2019) RNAcentral: A hub of information for non-coding RNA sequences. *Nucleic Acids Research*, 47, D221–D229.

Torchetti, E.M., Pegoraro, M., Navarro, B., Catoni, M., Di Serio, F. & Noris, E. (2016) A nuclear-replicating viroid antagonizes infectivity and accumulation of a geminivirus by upregulating methylation-related genes and inducing hypermethylation of viral DNA. *Scientific Reports*, 6, 35101.

Tsushima, D., Adkar-Purushothama, C.R., Taneda, A. & Sano, T. (2015) Changes in relative expression levels of viroid-specific small RNAs and microRNAs in tomato plants infected with severe and mild symptom-inducing isolates of potato spindle tuber viroid. *Journal of General Plant Pathology*, 81, 49–62. Available from: https://doi.org/10.1007/s10327-014-0566-7

Wang, C., Wang, C., Zou, J., Yang, Y., Li, Z. & Zhu, S. (2019) Epigenetics in the plant–virus interaction. *Plant Cell Reports*, 38, 1031–1038.

Wang, X., Li, N., Li, W., Gao, X., Cha, M., Qin, L. et al. (2020) Advances in transcriptomics in the response to stress in plants. *Global Medical Genetics*. 7, 30–34. Available from: https://pubmed.ncbi.nlm.nih.gov/32939512

Wassenegger, M. & Dalakouras, A. (2021) Viroids as a tool to study RNA-directed DNA methylation in plants. *Cells*, 10, 1187. Available from: https://pubmed.ncbi.nlm.nih.gov/34067940

Wassenegger, M., Heimes, S., Riedel, L. & Sänger, H.L. (1994) RNA-directed de novo methylation of genomic sequences in plants. *Cell*, 76, 567–576.

Waters, A.J., Makarevitch, I., Noshay, J., Burghardt, L.T., Hirsch, C.N., Hirsch, C.D. et al. (2017) Natural variation for gene expression responses to abiotic stress in maize. *The Plant Journal*, 89, 706–717. Available from: https://doi.org/10.1111/tpj.13414

Wickham, H. (2011) ggplot2. *Wiley Interdisciplinary Reviews: Computational Statistics*, 3, 180–185.

Wilkins, O., Hafemeister, C., Plessis, A., Holloway-Phillips, M.M., Pham, G.M., Nicotra, A.B. et al. (2016) EGRINs (Environmental Gene Regulatory Influence Networks) in rice that function in the response to water deficit, high temperature, and agricultural environments. *The Plant Cell*, 28, 2365–2384. Available from: https://pubmed.ncbi.nlm.nih.gov/27655842

Wu, T.D. & Watanabe, C.K. (2005) GMAP: a genomic mapping and alignment program for mRNA and EST sequences. *Bioinformatics*, 21, 1859–1875.

Xia, C., Li, S., Hou, W., Fan, Z., Xiao, H., Lu, M. et al. (2017) Global transcriptomic changes induced by infection of cucumber (*Cucumis sativus* L.) with mild and severe variants of hop stunt viroid. *Frontiers in Microbiology*, 8, 8.

Xu, X., Wang, K., Pan, J. & Chen, X. (2019) Small RNA sequencing identifies cucumber miRNA roles in waterlogging-triggered adventitious root primordia formation. *Molecular Biology Reports*, 46, 6381–6389. Available from: https://doi.org/10.1007/s11033-019-05084-z

Xu, X., Zhong, C., Tan, M., Song, Y., Qi, X., Xu, Q. et al. (2020) Identification of MicroRNAs and their targets that respond to powdery mildew infection in cucumber by small RNA and degradome sequencing. *Frontiers in Genetics*, 11, 246.

Yaish, M.W. (2017) Editorial: epigenetic modifications associated with abiotic and biotic stresses in plants: an implication for understanding plant evolution. *Frontiers in Plant Science*, 8, 1983. Available from: https://doi.org/10.3389/fpls.2017.01983

Yang, Y., Saand, M.A., Huang, L., Abdelaal, W.B., Zhang, J. & Wu, Y. et al. (2021) Applications of multi-omics technologies for crop improvement. *Frontiers in Plant Science*, 12, 563953. Available from: https://doi.org/10.3389/fpls.2021.563953

Zenda, T., Liu, S., Dong, A., Li, J., Wang, Y. & Liu, X. et al. (2021) Omics-facilitated crop improvement for climate resilience and superior nutritive value. *Frontiers in Plant Science*, 12, 774994. https://doi.org/10.3389/fpls.2021.774994

Zhang, Z., Xia, C., Matsuda, T., Taneda, A., Murosaki, F., Hou, W. et al. (2020) Effects of host-adaptive mutations on Hop stunt viroid pathogenicity and small RNA biogenesis. *International Journal of Molecular Sciences*, 21, 7383.

Zheng, Y., Wang, Y., Ding, B. & Fei, Z. (2017) Comprehensive transcriptome analyses reveal that potato spindle tuber viroid triggers genome-wide changes in alternative splicing, inducible trans-acting activity of phased secondary small interfering RNAs, and immune responses. *Journal of Virology*, 91, e00247–17. Available from: https://pubmed.ncbi.nlm.nih.gov/28331096

Zheng, Y., Wu, S., Bai, Y., Sun, H., Jiao, C., Guo, S. et al. (2019) Cucurbit genomics database (CuGenDB): a central portal for comparative and functional genomics of cucurbit crops. *Nucleic Acids Research*, 47, D1128–D1136.

Zhu, Q.-H., Shan, W.-X., Ayliffe, M.A. & Wang, M.-B. (2016) Epigenetic mechanisms: an emerging player in plant-microbe interactions. *Molecular Plant-Microbe Interactions®*, 29, 187–196. Available from: https://doi.org/10.1094/MPMI-08-15-0194-FI

Štajner, N., Radišek, S., Mishra, A.K., Nath, V.S., Matoušek, J. & Jakše, J. (2019) Evaluation of disease severity and global transcriptome response induced by citrus bark cracking viroid, Hop latent viroid, and their co-infection in hop (*Humulus lupulus* L.). *International Journal of Molecular Sciences*, 20, 3154. Available from: https://pubmed.ncbi.nlm.nih.gov/31261625

SUPPORTING INFORMATION

Additional supporting information can be found online in the Supporting Information section at the end of this article.

How to cite this article: Márquez-Molins, J., Villalba-Bermell, P., Corell-Sierra, J., Pallás, V. & Gomez, G. (2023) Integrative time-scale and multi-*omics* analysis of host responses to viroid infection. *Plant, Cell & Environment*, 1–19. https://doi.org/10.1111/pce.14647